A set of hyper-viscoplastic critical state models with different friction mobilisation criteria

Davood Dadras-Ajirlou [*], Gustav Grimstad, Seyed Ali Ghoreishian Amiri, Steinar Nordal

PoreLab – Centre of Excellence (SFF), Department of Civil and Environmental Engineering, Norwegian University of Science and Technology (NTNU), Trondheim, Norway

ABSTRACT

The approach of thermodynamics with internal variables, known as hyperplasticity, is used to develop a set of hyper-viscoplastic clay models that comply with the critical state soil mechanics and isotache viscosity. Different friction criteria of Drucker-Prager, Mohr-Coulomb, and Matsuoka-Nakai have been considered, and their conjugate features in terms of friction mobilisation and inelastic flow direction are explored. One of the distinctions of the proposed hyper-viscoplastic models regarding the existing models is having a unique friction envelope at the critical state (the paradigm of critical state soil mechanics) while adopting versatile dynamic yield surfaces and inelastic flow rules. To achieve this importance, an emphasis has been put on the practice of the stress ratio tensor (the deviatoric stress tensor per the spherical effective stress) as an essential state variable of frictional material. Along the way, some consistencies with the results and insights of studies with the discrete element method (DEM) in the literature are reported and interpreted.

1. Introduction

As a frictional particulate material, soils can sustain loads by mobilising shearing resistance at the contacts between particles. This single fact is crucial in modelling the deformation and failure of soil.

Several true triaxial tests (e.g., Kirkgard and Lade (1993), Kumruzaman (2012), Lade and Musante (1978), Nakai et al. (1986), Prashant and Penumadu (2004), Prashant and Penumadu (2005b), Ye et al. (2014), Yong and McKyes (1971)) have demonstrated that the shear strength of soil is essentially anisotropic, i.e., it varies according to the relative orientation of loading and failure plane. In addition to verifying this important macroscale observation, various simulations by the discrete element method (DEM) have also unveiled interesting features about the behaviour of particulate media in the mesoscale. It has been revealed that stresses on the macroscale arise by developing "force chains" that are a self-organising, emergent, and inhomogeneous mobilisation mechanism of skeletal forces at inter-grains/aggregates contacts on the mesoscale (Hurley et al., 2016). Force chains comprise "weak and strong sub-networks" (Radjai et al., 1998). Strong sub-networks with "non-sliding" contacts are preferentially oriented towards the major principal stress direction and carry nearly the whole deviatoric stress, whereas weak sub-networks with "sliding contacts" are on average aligned perpendicular to the major principal stress direction

and contribute mainly to spherical effective stress (Radjai et al., 1998, Radjai and Azéma, 2009, Shi and Guo, 2018b). This phenomenon has been demonstrated in several DEM simulations of particulate systems under deviatoric strain or stress paths (e.g., Thornton and Zhang (2010), Karapiperis et al. (2020), Phusing et al. (2017), Shi and Guo (2018a), Liu et al. (2020)). This bimodal attribute of the frictional dissipation on the mesoscale could result in anisotropic shear strength for the particulate system (Radjai and Azéma, 2009). In this regard, DEM studies of Maeda et al. (2006) and Shi and Guo (2018a) notably showed that the ratio of principal stresses is approximately proportional to the square root of the corresponding proportion of the principal values of the so-called "fabric tensor" defined as an average of whole contact network in the particulate system after Satake (1982) and Oda (1993).

Our mesoscopic speculation regarding the development of force chains in clay (extending the notion from perfect granule to clay) is bound to the idealisation that the clay skeleton is an assembly of aggregates (analogy grains) made of many thousands of clay platelets (e.g., Chang et al. (2009), Hattab and Chang (2015), Hicher et al. (2000)). Of course, microscopically, the situation is significantly more complex for clay as these relatively large aggregates are soft or crushable affecting the transfer of stress between their contacts inside the skeleton. Further complexity comes from the physicochemical interactions in clay. Apart from these extra complexities and as a worthy excursion from the main theme, this paper attempts to remark on the plausible physical

---

Abbreviations: CSSM, Critical State Soil Mechanics; DEM, Discrete Element Method; DKP, Dual Kinematic Plane; DP, Drucker-Prager; HKMD, Hong Kong Marine Deposits; MC, Mohr-Coulomb; MN, Matsuoka-Nakai; OCR, Over Consolidation Ratio; SMP, Spatially Mobilised Plane.

* Corresponding author.

E-mail address: davood.dadrasajirlou@ntnu.no (D. Dadras-Ajirlou).

Nomenclature

f	Helmholtz free energy potential
G	Shear modulus
g	Dimensionless shear modulus coefficient
$I_1, I_2,$ and I_3	The first, second and third invariants of Cauchy stress tensor $\boldsymbol{\sigma}$
K	Bulk modulus
M	frictional coefficient
n	Homogeneity degree of force potential or rate sensitivity parameter
OCR	Over consolidation ratio
p	spherical effective stress
p_0	isotropic pre-consolidation pressure
p_a	Reference pressure (atmospheric pressure) in Helmholtz free energy potential
p_{eq}	Equivalent pressure on isotropic unloading reloading line (IURL)
p_{ref}	Reference pressure for definition of p_0
q	Deviatoric stress invariant

R	Spacing ratio
r	Norm of an arbitrary reference volumetric strain rate
S	State variable
T	Transition function
w	Flow potential
z	Force potential
υ	Specific volume
$\boldsymbol{\varepsilon}, \boldsymbol{\varepsilon}^p$	Total and inelastic strain tensor
$^{D}\boldsymbol{\varepsilon}, {}^{D}\boldsymbol{\varepsilon}^p$	Total and inelastic deviatoric strain tensor
$\varepsilon_v, \varepsilon_v^p$	Total and inelastic volumetric strain
φ_{CS}	Critical state angle of shearing resistance
γ	Parameter for the frictional dissipation
$\boldsymbol{\eta}$	Stress ratio tensor
θ	Lode angle
κ	Slope of isotropic unloading reloading line (IURL)
λ	Slope of normal compression line (NCL)
μ	Creep index
χ_p, χ_q	spherical and deviatoric invariants of dissipative stress tensor

mesoscopic mechanism behind the Lode angle dependent behaviour, a matter that has previously been treated in a purely algebraic manner. To do so, we appeal to the insights gained by DEM studies with "ideal granules". This may be justified by the absence of representative real and virtual experiments on clay targeting the Lode angle dependency of its behaviour, besides the nature of coulomb friction between particulate constituents of frictional media. Furthermore, the formation of force chains in soft gels (Vinutha et al., 2023, Dong et al., 2022) with similar morphology to clay implies the possibility of a similar phenomenon occurring in clay.

The insights gained by DEM simulations generally support the continuum-based concept of "Spatially Mobilised Plane" (SMP) (Matsuoka and Nakai, 1974) and subsequently the Matsuoka-Nakai (MN) friction theory. The MN friction theory later led to the development of the modified stress concept (t_{ij} concept) (Nakai, 2007, Nakai and Mihara, 1984) to describe the mechanical behaviour of soils in general three-dimensional stress conditions. The MN friction has been engaged with the critical state soil mechanics (CSSM) (Schofield and Wroth, 1968) by using the plasticity theory and subsequently led to a few continuum constitutive models that can successfully capture the general shear and compression behaviour of soils (Matsuoka, 2006, Nakai, 2012). In a different line of thought, Collins (2003), based on the works by Houlsby (1981) and Collins and Houlsby (1997a), provides a detailed procedure for consideration of the MN friction in the families of critical state models using the hyperplasticity approach.

Recently Dadras-Ajirloo et al. (2022), by using the hyperplasticity approach (Houlsby and Puzrin, 2007) and subscribing to the CSSM and the isotache viscosity (Leroueil, 2006, Suklje, 1957), have developed a constitutive model for describing the creep and rate-dependent behaviour of clay. The model is formulated by specifying two thermodynamic potentials, namely the force and the free energy potentials. It enjoys the non-associated flow rule as a natural consequence of including the frictional dissipative mechanism (Collins and Kelly, 2002) while securing a unique critical state envelope. However, by following Roscoe and Burland (1968), the model is developed for the simple condition of isotropic friction mobilisation being independent of the shearing mode (Lode angle dependency). The primary purpose of the current paper is to generalise the developed hyper-viscoplastic model to consider the anisotropic nature of friction mobilisation by employing the MN friction criterion. Along the way, some interesting consistencies with DEM observations and insights are also reported.

Several experimental studies (e.g., Adachi et al. (1995), Arulanandan

et al. (1971), Sheahan et al. (1996), Vaid and Campanella (1977), Zhu (2000), Tafili et al. (2021)) have demonstrated that the mobilised friction at critical state does not significantly depend on the loading rate. This experimental finding is supporting the fact that the coulomb sliding friction (macro-scale) is approximately independent of the rate of mechanical processes. This is ideally equivalent to the uniqueness of the critical friction envelope under different loading rates. However, it has come to the authors' attention that in the trend of the viscoplastic, critical state constitutive modelling of soil behaviour using the hyperplasticity approach, the uniqueness of the mobilised friction at the critical state is not respected (e.g. Jacquey and Regenauer-Lieb (2021)). A unique envelope for the mobilised friction at the critical state is an essential paradigm in the CSSM for a unified description of the general mechanical behaviour (shear and consolidation) of soils. In this regard, Grimstad et al. (2020) and Grimstad et al. (2021) have pointed out the possible formulations for the non-uniqueness of the critical friction envelope. The current paper also explores these ill formulations considering the MN friction criterion. Moreover, a sophisticated force potential coupled with the friction mobilisation criteria is proposed to achieve a versatile dynamic yield surface (Perzyna, 1963) and flow rule while securing a unique friction envelope at the critical state (frictional failure envelope).

Lastly, the efficacy of the proposed hyper-viscoplastic model is evaluated by simulating the triaxial and the true triaxial tests conducted on the Hong Kong Marine Deposit (HKMD) (Zhu, 2000) and the Fujinomori clay (Nakai et al., 1986).

2. Nomenclatures and assumptions

The hyperplasticity approach (Houlsby and Puzrin, 2006) is a systemized version of the approach of Ziegler (1983) with unconditional thermodynamics consistency including the principle of maximum energy dissipation rate. In this approach, all elements of a constitutive model such as yield and plastic potential surfaces, hardening rules and elasticity are defined through the specification of two potentials: the free energy potential and the dissipation function (or force potential). The free energy potential describes the conservative and path-independent behaviour, whilst the dissipation function expresses the dissipative and path-dependent behaviour. The detailed context of the hyperplasticity approach for modelling the inelastic viscous behaviour can be found in Houlsby and Puzrin (2002) and Houlsby and Puzrin (2007). The concise account of hyperplasticity formalism is provided in a

collection of Appendices with notations and terminologies similar to Houlsby and Puzrin (2007).

Following the conventional practice, the total strain ($\boldsymbol{\varepsilon}$) and inelastic strain ($\boldsymbol{\varepsilon}^\mathrm{p}$, known as the internal variable), are taken as the kinematic variables of the system. All stresses (dependent variables) are effective stresses, and compressive strains and stresses are positive. The formulations are strain-based with the assumption of infinitesimal strain in the Cartesian coordinate system for the isothermal processes. Therefore, the viscoplastic constitutive model is preferably expressed in terms of the Helmholtz free energy and the force potential. It is also assumed that the elastic stiffness of the material is decoupled, meaning elastic moduli are independent of the internal variable (inelastic strain).

In the current work, boldface characters will denote second-order tensor quantities. All tensor quantities are symmetric. The trace of an arbitrary second-order tensor $\boldsymbol{x} = x_{ij}\widehat{e}_i \otimes \widehat{e}_j$, where the symbol '$\otimes$' stands for the dyadic or tensor product between the Cartesian bases $\{\widehat{e}_i\}$, is defined as $\mathrm{tr}(\mathbf{x}) = x_{ii}$ in which the summation convention over repeated indices is employed. Thus, the deviatoric component of an arbitrary second-order tensor ($^D\boldsymbol{x}$) is:

$$^D\boldsymbol{x} = \boldsymbol{x} - \left(\frac{tr(\boldsymbol{x})}{3}\right)\mathbf{1} \tag{1}$$

where $\mathbf{1} = \delta_{ij}\widehat{e}_i \otimes \widehat{e}_j$ the second-order identity tensor with components δ_{ij}, the Kronecker delta, relative to a Cartesian coordinate system. If $\times = \boldsymbol{\sigma}$, $\mathrm{tr}(\boldsymbol{x})/3$ is the spherical effective stress denoted by p in the following. The symbol ':' between two tensor quantities denotes the double index contraction of their product, e.g., in cartesian axes between two second-order tensors $\boldsymbol{a} : \mathbf{b} = a_{ij}b_{ij}$. The composition of two arbitrary second-order tensors is defined as $\boldsymbol{a}.\boldsymbol{b} = a_{ik}b_{kj}\widehat{e}_i \otimes \widehat{e}_j$. Therefore, the trace of a composition of two arbitrary second-order tensors becomes $\mathrm{tr}(\mathbf{a}.\mathbf{b}) = a_{ij}b_{ji}$

3. Helmholtz free energy

The proposed model employs the Helmholtz form (f) of the free energy potential developed by Houlsby et al. (2005):

$$f = \kappa p_a \exp\left(\frac{\mathrm{tr}(\boldsymbol{\varepsilon} - \boldsymbol{\varepsilon}^\mathrm{p}) + g\mathrm{tr}((\mathrm{D}\boldsymbol{\varepsilon} - \mathrm{D}\boldsymbol{\varepsilon}^\mathrm{p})^2)}{\kappa}\right) \tag{2}$$

where κ and g are dimensionless material parameters defining the elastic bulk and shear moduli, respectively. p_a is an arbitrary reference pressure (preferably $p_\mathrm{a} = 100$ kPa).

The Helmholtz free energy describes the path-independent and reversible behaviour of the material. In addition to being strictly convex, it is reference independent and suitable for modelling long-term creep and relaxation (Dadras-Ajirloo et al., 2022). This importance enables the laboratory-estimated material viscous parameters (to be defined in the following) to be representative of the material under the in situ condition with a significantly different time scale (Jostad and Yannie, 2017, Bjerrum, 1967).

Equation (2) is also a positive definite function for any material state, meaning that positive work must be done on the material to deform. Moreover, the deviatoric and volumetric components of the strain tensor are coupled via an exponential function to provide spherical effective stress-dependent elastic moduli (a common feature for geomaterials). This later feature results in an induced anisotropy imposed by the first law (Amorosi et al., 2020, Houlsby et al., 2005).

The fourth-order symmetric elasticity tensor D can be derived as:

$$D = \frac{\partial^2 f}{\partial \boldsymbol{\varepsilon} \otimes \partial \boldsymbol{\varepsilon}} = \left(\frac{1}{\kappa p}\right)\boldsymbol{\sigma} \otimes \boldsymbol{\sigma} + 2gp\left[\mathrm{I} - \frac{1}{3}\mathbf{1} \otimes \mathbf{1}\right] \tag{3}$$

where $\mathrm{I} = \frac{1}{2}\left[\delta_{ik}\delta_{jl} + \delta_{il}\delta_{jk}\right]\widehat{e}_i \otimes \widehat{e}_j \otimes \widehat{e}_k \otimes \widehat{e}_l$ is the fourth-order symmetric identity tensor. For isotropic stress states, the bulk modulus (K) becomes:

$$K = \frac{p}{\kappa} \tag{4}$$

indicating that κ is the slope of the isotropic drained unloading line in the bi-logarithmic compression plane of $\ln(v)$-$\ln(p)$ with v being the specific volume.

Another prime feature of the employed free energy potential is the lack of pure plastic part in the free energy. In the hyperplastic description of the MCC model (Collins, 2003, Collins and Hilder, 2002, Collins and Kelly, 2002), the plastic free energy is exclusively dependent on the volumetric component of the internal variable, which results in a "shift" or "back" spherical stress. Based on Collins (2005), the nonstorage of the volumetric plastic work (zero shift stress) can be interpreted as homogenous volumetric mechanisms in the lower (meso) scale. Grimstad et al. (2020) have demonstrated that this choice can secure a unique critical friction envelope for a rate-dependent system with a single internal variable under different loading rates.

4. Classical force and flow potentials

To integrate the MN friction in hyper-viscoplastic models and to investigate its features, it is convenient to embark on the force potential (z) proposed by Grimstad et al. (2020) and Dadras-Ajirloo et al. (2022). This force potential is based on two phenomenological concepts of the critical state (Schofield and Wroth, 1968) and the isotache viscosity (Suklje, 1957). It is expressed as:

$$z = \frac{rp_0}{n}\left(\frac{\sqrt{\mathrm{tr}^2(\dot{\boldsymbol{\varepsilon}}^\mathbf{p}) + (\overline{\mathbf{M}}\overline{\dot{\boldsymbol{\varepsilon}}}_\mathbf{s}^\mathbf{p})^2} + \mathrm{tr}(\dot{\boldsymbol{\varepsilon}}^\mathbf{p})}{2r}\right)^n \tag{5}$$

To achieve a comprehensive dissipative mechanism, according to Roscoe and Burland (1968), the compressional and shearing dissipative mechanism are coupled via the Euclidean norm of the trace of inelastic strain rate (volumetric strain rate) and a certain norm form of inelastic shear strain rate ($\overline{\dot{\varepsilon}}_s^p$) weighted by the corresponding frictional coefficient $\overline{M}$. In this paper, the terms characterised by a bar, all of which are associated with a shearing process, are to be suited for an intended frictional criterion.

p_0 in equation (5) is the isotropic pre-consolidation pressure. The evolution of p_0 in an inelastic process renders the material resistance against further compression or creep (soil's memory). According to the CSSM, p_0, which its evolution is known as isotropic hardening, can be expressed as:

$$p_0 = p_{ref}\exp\left(\frac{tr(\boldsymbol{\varepsilon}^p)}{\lambda - \kappa}\right) \tag{6}$$

where p_ref is the value of p_0 at zero inelastic volumetric strain, κ is defined in equation (4), and λ is the slope of normal compression behaviour on the bi-logarithmic plane of $\ln(v)$-$\ln(p)$.

The force potential (equation (5)) is non-negative definite with the positive homogeneity degree of $n \geqslant 1$. The isotache viscosity, based on which a unique relation between effective stress, strain (or specific volume), and strain rate exists (Leroueil, 2006, Suklje, 1957), is considered by scaling a reference inelastic (creep) power equal to r times p_0. The parameter r depicts the trace (volumetric component) of a reference inelastic strain rate associated with p_0. The scaling is performed by the rate sensitivity parameter or viscosity index ($n \geqslant 1$), which controls the degree of positive homogeneity of the force potential and regulates the spacing between so-called isotaches, i.e., contours of stress–strain each associated with a certain rate. By following Janbu's time resistance concept (Janbu, 1969, Janbu, 1985), it has been demonstrated that n can be slightly larger than one (Grimstad et al., 2010):

$$n = 1 + \frac{\mu}{\lambda - \kappa} \tag{7}$$

where μ is the creep index that can be objectively quantified using the time resistance concept (Grimstad et al., 2015, Jostad and Yannie, 2017). For $\mu = 0 \rightarrow n = 1$, the force potential becomes rate-independent (positively homogenous of degree one), leading to one of two forms of MCC dissipation function (Houlsby, 2000). For further discussion and details about the force potential (equation (5)), refer to Dadras-Ajirloo et al. (2022).

By following the procedure explained by Grimstad et al. (2020), the flow potential (w), which provides the evolution of the internal variable, can be expressed as:

$$w = r p_0 \left(\frac{n-1}{n} \right) \left(\frac{p_{eq}}{p_0} \right)^{\frac{n}{n-1}} \tag{8}$$

where p_{eq} is the equivalent isotropic stress measure in the dissipative stress space and resembles the size of the dynamic yield surface (Perzyna, 1963). It is defined as:

$$p_{eq} = \chi_p \left[1 + \left(\frac{\overline{\chi}_q}{\overline{M}\chi_p} \right)^2 \right] \tag{9}$$

χ_p is the spherical dissipative stress work conjugated to volumetric inelastic strain rate. $\overline{\chi}_q$ is a norm form of deviatoric dissipative stress work conjugated to the chosen $\overrightarrow{\varepsilon}_s^p$. According to equation (8), the degree of positive homogeneity of the flow potential w with respect to the dissipative stress is obtained to be $n/(n-1)$, which is confirmed by the scaling property of Legendre-type homogeneous functions (see Appendix B and Appendix E).

In the following, the focus is placed on the integration of the MN friction criterion with the isotache hyper-viscoplastic critical state model through the specification of $\overrightarrow{\varepsilon}_s^p$, $\overline{M}$, and $\overline{\chi}_q$. The conventional friction criteria of the Drucker-Prager (DP) and the DP with Lode angle dependency, which is commonly practised in the plasticity theory as the Mohr-Coulomb (MC), are also introduced for effective appreciation of the features of the MN friction.

The MN friction is derived from the continuum-mechanics-based concept of SMP. Matsuoka (1976) interprets the SMP as the plane with the most mobilised grains/aggregates. This physically appealing hypothesis has been alluded to by several DEM studies (e.g., Maeda et al. (2006), Shi and Guo (2018b), Fleischmann (2020), Zhou et al. (2021)). The SMP can be characterised by the unit norm tensor of $\sqrt{\boldsymbol{\sigma}^{-1}/\boldsymbol{tr}(\boldsymbol{\sigma}^{-1})}$, and the mobilised friction on the SMP (the MN friction), that is, the ratio of shear stress to normal stress on the SMP (η_{SMP}), can be cast as:

$$\eta_{SMP} = \sqrt{p \operatorname{tr}(\boldsymbol{\sigma}^{-1}) - 3} = \sqrt{\frac{I_1 I_2}{3 I_3} - 3} \tag{10}$$

where I_1, I_2 and I_3 are the first, second and third stress invariants which are expressed as:

$$I_1 = \operatorname{tr}(\boldsymbol{\sigma}) = \sigma_1 + \sigma_2 + \sigma_3$$

$$I_2 = \frac{1}{2} \left[\operatorname{tr}^2(\boldsymbol{\sigma}) - \operatorname{tr}(\boldsymbol{\sigma}^2) \right] = \sigma_1 \sigma_2 + \sigma_2 \sigma_3 + \sigma_3 \sigma_1 \tag{11}$$

$$I_3 = \frac{1}{6} \left[\operatorname{tr}^3(\boldsymbol{\sigma}) - 3\operatorname{tr}(\boldsymbol{\sigma})\operatorname{tr}(\boldsymbol{\sigma}^2) + 2\operatorname{tr}(\boldsymbol{\sigma}^3) \right] = \sigma_1 \sigma_2 \sigma_3$$

where σ_1, σ_2, and σ_3 are principal stresses. Failure in the MN friction criterion is assumed to occur when η_{SMP} approaches a unique value denoted here by M_{SMP} representing the particulate system's macro-scale friction at the critical state, which can be cheaply quantified by triaxial or other shear tests. By composing the unit norm normal tensor of $\sqrt{\boldsymbol{\sigma}^{-1}/\boldsymbol{tr}(\boldsymbol{\sigma}^{-1})}$ with the Cauchy stress tensor $\boldsymbol{\sigma}$, Nakai and Mihara (1984) transformed $\boldsymbol{\sigma}$ into a so-called modified stress tensor. Based on the

plasticity theory, they adopted the MN friction in the critical state models. Nakai (2007) interprets this mapping process as a consideration of the stress-induced anisotropy originating from the development of the strong (on SMP) and weak force chains, which is called the force anisotropy by Radjai and Azéma (2009).

As another prime development in this direction, Collins (2003) brought the MN friction to the critical state models using the hyperplasticity approach. To do so, Collins (2003) defined the dual form of the SMP called "Dual Kinematic Plane" (DKP), characterised by the unit norm tensor of $\sqrt{\boldsymbol{\sigma}/\operatorname{tr}(\boldsymbol{\sigma})}$ to maintain the work-conjugacy of variables which is the fundamental premise of the hyperplasticity framework. In contrast to Nakai and Mihara (1984) but under the same assumption of the coaxiality between the stress $\boldsymbol{\sigma}$ and the inelastic strain rate $\dot{\boldsymbol{\varepsilon}}^p$ tensors, Collins (2003) composed the characteristic tensor of the DKP with $\dot{\boldsymbol{\varepsilon}}^p$ and proposed the following shear strain rate measure on the DKP:

$$\dot{\varepsilon}_{s,DKP}^p = \frac{\sqrt{\operatorname{tr}(\boldsymbol{\sigma})\operatorname{tr}\left(\boldsymbol{\sigma}.\left(^{D}\dot{\boldsymbol{\varepsilon}}^p\right)^2\right) - \left(\operatorname{tr}\left(\boldsymbol{\sigma}.\,^{D}\dot{\boldsymbol{\varepsilon}}^p\right)\right)^2}}{\operatorname{tr}(\boldsymbol{\sigma})} \tag{12}$$

The classical isotache hyper-viscoplastic model with the MN friction criterion can be achieved by employing $\dot{\varepsilon}_{s,DKP}^p$. After replacing $\overrightarrow{\varepsilon}_s^p = \sqrt{3}\dot{\varepsilon}_{s,DKP}^p$ (merely for the sake of consistency with Collins (2003)) and $\overline{M} = M_{SMP}$ in the force potential, the flow potential can be derived as (see Appendix F):

$$\begin{aligned} w_{\text{SMP}} &= \left(\frac{n-1}{n} \right) (r p_0) \left(\frac{\chi_p}{p_0} \left(1 + \left(\frac{\sqrt{p \operatorname{tr}\left(\boldsymbol{\sigma}^{-1}.\left(^{D}\boldsymbol{\chi}\right)^2\right)}}{M_{SMP}\chi_p} \right)^2 \right) \right)^{\frac{n}{n-1}} \\ &= \left(\frac{n-1}{n} \right) (r p_0) \left(\frac{p_{eq}}{p_0} \right)^{\frac{n}{n-1}} \end{aligned} \tag{13}$$

Since there is no pure plastic free energy and subsequently no shift stress (back stress), thus based on Ziegler's orthogonality postulate, the dissipative stress tensor $\boldsymbol{\chi}$ is equal to the true stress (Cauchy stress) tensor $\boldsymbol{\sigma}$. Therefore, after some simplification, p_{eq} in equation (13) can be written in the true stress space as:

$$p_{eq} = p \left(1 + \frac{p \operatorname{tr}(\boldsymbol{\sigma}^{-1}) - 3}{M_{SMP}^2} \right) = p \left(1 + \left(\frac{\eta_{SMP}}{M_{SMP}} \right)^2 \right) \tag{14}$$

Similarly, the shear strain rate on the octahedral plane can be cast from the composition of the unit norm characteristic tensor of $\sqrt{1/\operatorname{tr}(\mathbf{1})}$ and $^{D}\dot{\boldsymbol{\varepsilon}}^p$ whose norm is:

$$\dot{\varepsilon}_{s,OCT}^p = \sqrt{\frac{\operatorname{tr}\left(\mathbf{1}.\left(^{D}\dot{\boldsymbol{\varepsilon}}^p\right)^2\right)}{\operatorname{tr}(\mathbf{1})}} = \sqrt{\frac{\operatorname{tr}\left(\left(^{D}\dot{\boldsymbol{\varepsilon}}^p\right)^2\right)}{3}} \tag{15}$$

For this case, by taking $\overrightarrow{\varepsilon}_s^p = \sqrt{2}\dot{\varepsilon}_{s,OCT}^p$ and $\overline{M} = M_{OCT}$ in the force potential (equation (5)), the classical isotache hyper-viscoplastic model (Grimstad et al. (2020), Dadras-Ajirloo et al. (2022)) with the DP friction criterion can be obtained. w for this case can be expressed as:

$$\begin{aligned} w_{OCT} &= \left(\frac{n-1}{n} \right) (r p_0) \left(\frac{\chi_p}{p_0} \left(1 + \left(\frac{\sqrt{\frac{3}{2} tr\left(\left(^{D}\boldsymbol{\chi}\right)^2\right)}}{M_{OCT}\chi_p} \right)^2 \right) \right)^{\frac{n}{n-1}} \\ &= \left(\frac{n-1}{n} \right) (r p_0) \left(\frac{p_{eq}}{p_0} \right)^{\frac{n}{n-1}} \end{aligned} \tag{16}$$

which after the transformation of $\boldsymbol{\chi} = \boldsymbol{\sigma}$, p_{eq} can be written as:

$$p_{eq} = p \left(1 + \frac{3 tr\left(\left(^{D}\boldsymbol{\sigma}\right)^2\right)}{2 p^2 M_{OCT}^2} \right) = p \left(1 + \left(\frac{\eta_{OCT}}{M_{OCT}} \right)^2 \right) \tag{17}$$
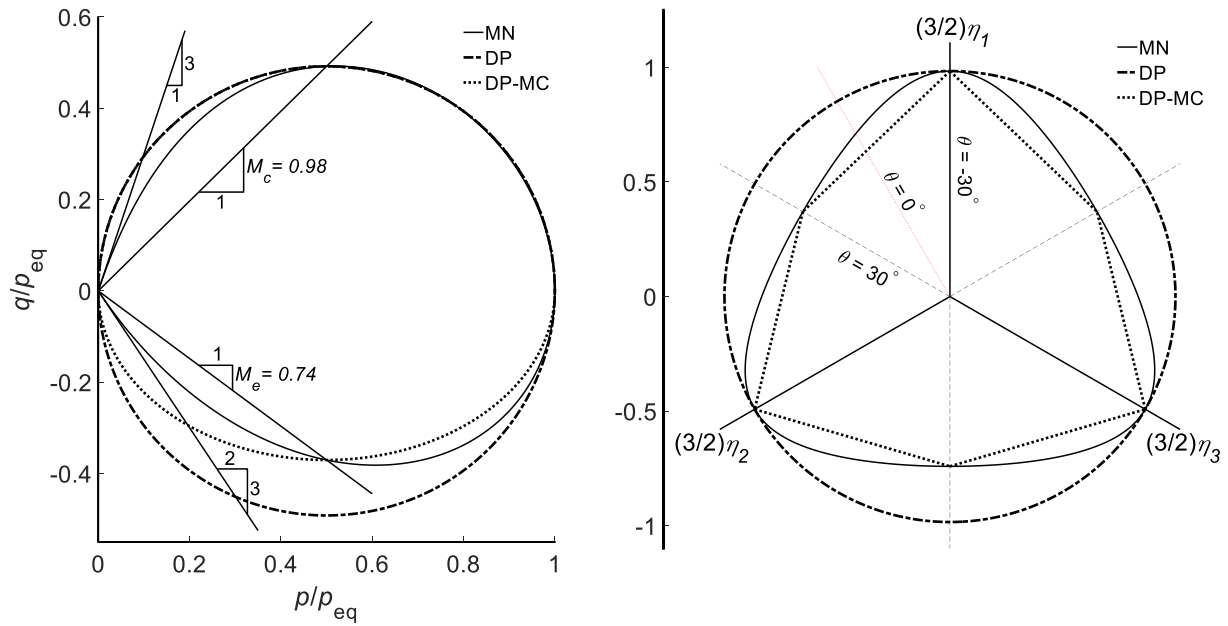
Fig. 1. (a) Dynamic yield surfaces and (b) the corresponding mobilised friction at critical state according to different friction criteria for friction criteria of Drucker-Prager (DP), conventional Mohr-Coulomb (DP-MC), and Matsuoka-Nakai (MN) when $\varphi = 25°$- Note that the left side scale in (b) is a metric for the stress ratio (representative of friction) at critical state in one out of three possible situations for axisymmetric loading.

Similarly, the common form of the MC friction in plasticity theory can also be simply accommodated by taking the same measure of dissipative shear strain rate on the octahedral plane ($\bar{\dot{\varepsilon}}_s^p = \sqrt{2}\dot{\varepsilon}_{s,OCT}^p$) and adapting the frictional coefficient $\overline{M}$ as:

$$\overline{M} = \frac{3\sin(\varphi_{cs})}{\sqrt{3}\cos(\theta) + \sin(\theta)\sin(\varphi_{cs})} \tag{18}$$

where φ_{cs} represents the critical state angle of shearing resistance of the particulate system at the macroscale. θ stands for the Lode's angle defined as:

$$\theta = -\frac{1}{3}\sin^{-1}\left(\sqrt{6}\,tr(e_\theta^3)\right)$$
$$e_\theta = \frac{\eta}{\sqrt{tr(\eta^2)}} \tag{19}$$

where $\eta = {}^D\sigma/p$ is the stress ratio tensor.

It is essential to recognise that the shear dissipation on the non-evolving octahedral plane led to the friction mobilisation (η_{OCT}) on the very same plane for the DP and the MC. The only difference is that for the MC case, the frictional coefficient varies with the Lode's angle due to the directional variation of η. Consequently, the MC will be renamed DP-MC from now on. On the other hand, for the MN, shearing dissipation on the evolving DKP resulted in friction mobilisation on the evolving SMP (η_{SMP}). In fact, by employing equation (15), the dissipative shear strain rate measure on the DKP (equation (12)) becomes:

$$\dot{\varepsilon}_{s,DKP}^p = \sqrt{\left(\dot{\varepsilon}_{s,OCT}^p\right)^2 + \frac{1}{3}tr(\eta.({}^D\dot{\varepsilon}^p)^2) - \left(\frac{1}{3}tr(\eta.({}^D\dot{\varepsilon}^p))\right)^2} \tag{20}$$

DEM studies (e.g. Radjai et al. (1998), Alonso-Marroquín et al. (2005), Antony and Kruyt (2009) and Radjai and Azéma (2009)) imply that the stress ratio η could represent the degree of the bimodal dissipative behavioural feature of particulate systems (development of the strong and weak force chains). It has been numerously demonstrated that the strong force chains carry almost the entire deviatoric stress while the weak force chains contribute only to the spherical stress.

Interestingly, a bimodal behaviour under conventional axisymmetric loading has been observed in a real experiment on kaolin clay as well, in which even the orientation and arrangement of clay aggregates are affected (Hattab, 2011). Based on equation (20), as η increases and the bimodal behaviour intensifies, the dissipative shear strain rate deviates from the dissipative strain rate on the stationary octahedral plane. The consequence of this deviation (stress-induced anisotropy) in terms of friction mobilisation and the corresponding inelastic flow is explored in the following sections.

It is worth noting that the meaning of friction is more than the mere slide of particles passing each other. Here, the mobilised friction in the macro-scale is considered as a norm of stress ratio depending on macro/meso physical entities such as the voids, the distribution of contacts and the interlocking between aggregates besides the friction between them. The CSSM phenomenologically tries to tie all these interacting entities by linking the consolidation and shearing behaviour.

It should also be pointed out that the following results and observations on friction mobilisation and inelastic flow direction for the DP-MC friction criterion can be extended to other convex deviatoric shape functions (e.g. Van Eekelen (1980) and Panteghini and Lagioia (2018)) since their hyperplastic implementations are the same as the DP-MC criterion.

5. Friction mobilisation

For clarity and simplicity, the following visualisations have been done in the normalised triaxial q/p_{eq}-p/p_{eq} plane with $q = \sigma_1 - \sigma_3$ and $p = (\sigma_1 + 2\sigma_3)/3$. q is the deviatoric stress measure under the axisymmetric condition ($\sigma_2 = \sigma_3$) comprising triaxial compression ($\sigma_1 \gg \sigma_2 = \sigma_3$) and extension ($\sigma_2 = \sigma_3 \gg \sigma_1$). Moreover, for a better visual interpretation of the friction mobilisation, the mobilised friction is illustrated in terms of the stress ratio for each criterion on the deviatoric or so-called π-plane (the octahedral plane on which the spherical stress is zero) in the Haigh-Westergaard stress space.

Fig. 1 illustrates the dynamic surfaces (Fig. 1a) and the corresponding mobilised friction at the critical state (deviatoric failure surface) (Fig. 1b) according to different friction criteria on the normalised triaxial and the π-plane. For comparison, the critical state in the
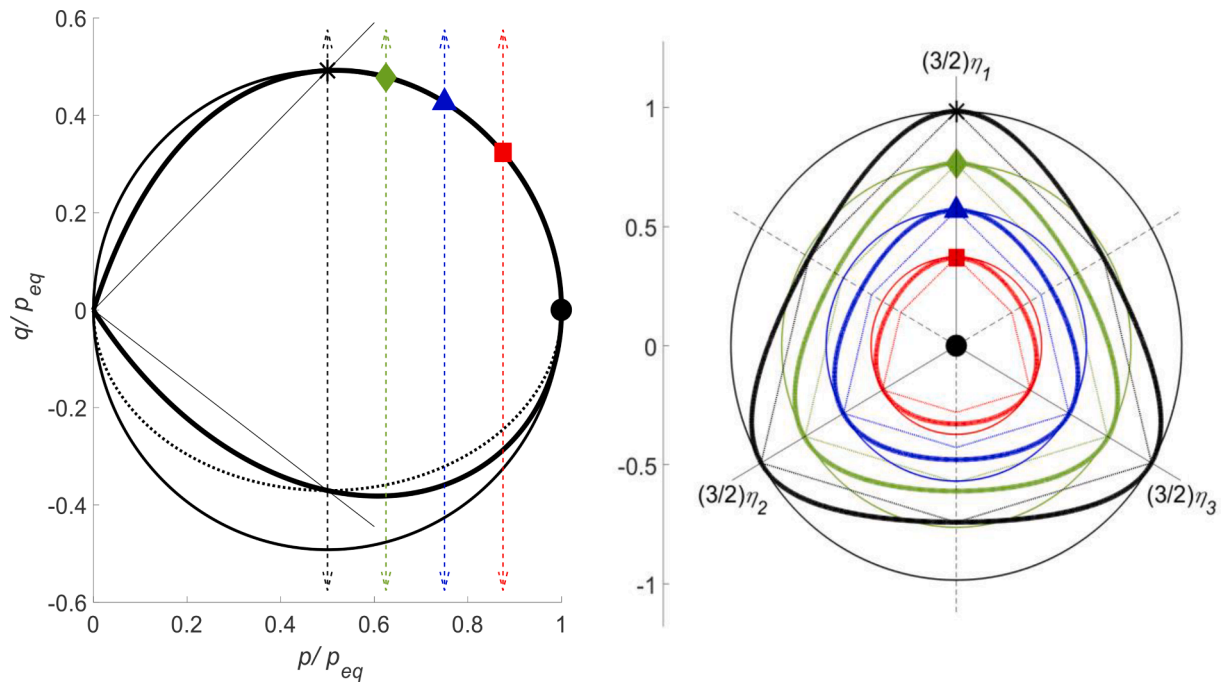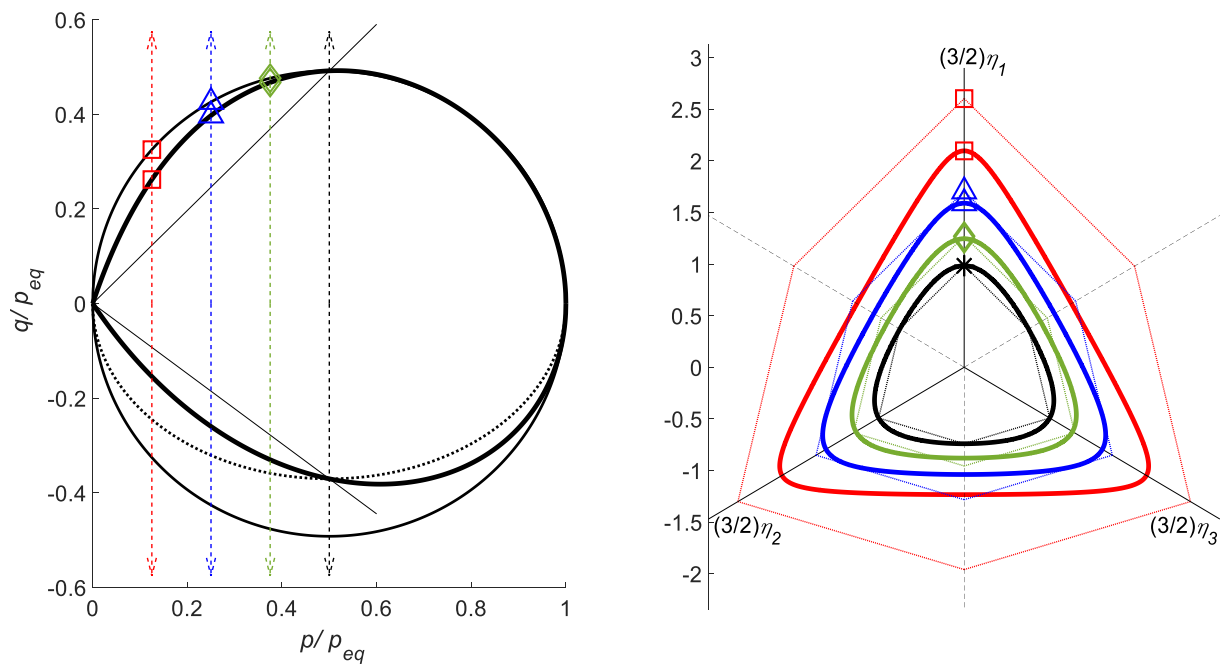
Fig. 2. Friction mobilisation for the states on the looser side of the critical friction envelope: (a) representative states, (b) Drucker-Prager (DP), the conventional Mohr-Coulomb (DP-MC), and Matsuoka-Nakai (MN) friction envelope at the representative states when $\varphi = 25°$- Note that the left side scale in (b) is a metric for the stress ratio (representative of friction) at critical state in one out of three possible situations for axisymmetric loading.

axisymmetric compression ($\theta = -30°$) for all friction criteria is chosen to be the same. This unique failure state for different friction criteria has been achieved by adjusting M_{SMP} and M_{OCT} as:

$$M_{OCT} = M_C(\theta = -30°) = \frac{6\sin(\varphi_{cs})}{3 - \sin(\varphi_{cs})} \tag{21}$$

$$M_{SMP} = 2\sqrt{\frac{2}{3}}\tan(\varphi_{cs}) \tag{22}$$

The comparison of the convex dynamic surfaces associated with different friction criteria in Fig. 1(a) demonstrates that the MN dynamic surface is not elliptical but more distorted, particularly in the axisymmetric extensional region. On the right side of the critical state line in the axisymmetric compressional region, where the soil is known to be in a looser state, the friction mobilisation (here in terms of triaxial stress ratio q/p) for all criteria is almost identical. Indeed, it is the same for the DP and DP-MC, but with a minor difference for the MN depending on the value of φ_{cs}. However, on the left side of the critical state line in triaxial

Fig. 3. Friction mobilisation for the states on denser side of the critical friction envelope: (a) representative states, (b) Drucker-Prager (DP), the conventional Mohr-Coulomb (DP-MC), and Matsuoka-Nakai (MN) friction envelope at the representative states when $\varphi = 25°$- Note the left side scale in (b) is a metric for the stress ratio (representative of friction) at critical state in one out of three possible situations for axisymmetric loading.
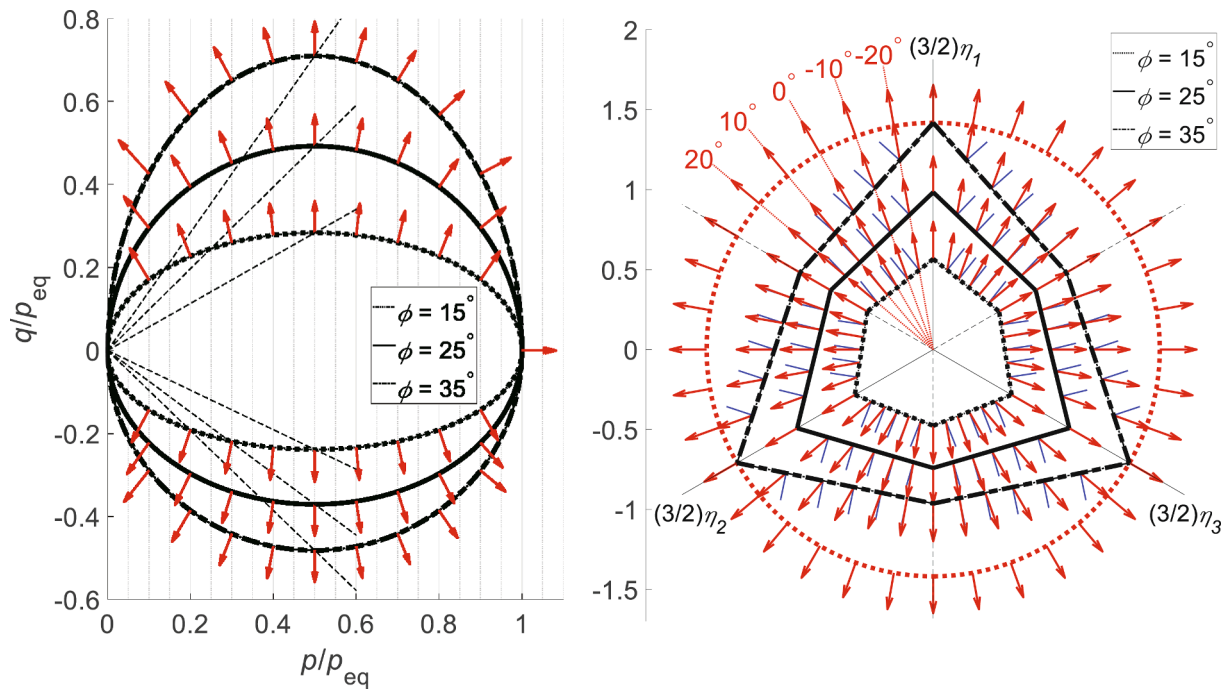
Fig. 4. Dynamic surfaces and the corresponding inelastic flow directions on (a) the normalised meridian plane and (b) the deviatoric plane at the critical state for the conventional Mohr-Coulomb (DP-MC) friction criterion when $\varphi = 15°$, $25°$, and $35°$. Note that the vectors without arrows next to each inelastic flow vectors are the gradient of the deviatoric surface. Moreover, the left side scale in (b) is a metric for the stress ratio (representative of friction) at the critical state in one out of three possible situations for axisymmetric compression.

compression and extension, where the soil state is relatively denser (existence of interlocking between grains/aggregates), the MN friction mobilisation considerably deviates from the DP-MC and the DP. The dynamic surface with the MN friction becomes tangential to the dashed lines called tension cut-off as the stress state approaches the origin. The tension cut-off lines with a slope of 1:3 for compression and 2:3 for extension separate the stress states with negative values of the principal stresses under axisymmetric conditions. As a result of this deviation, the states at which the principal stresses are negative are not attainable. On the extensional looser side, the MN friction mobilises towards the critical friction in such a way that deviates from the DP and approaches the DP-MC at the critical state.

According to Fig. 1(b), the isotropic friction criterion of DP gives the same critical friction as the axisymmetric compression for any deviatoric loading directions. On the other hand, the mobilised friction at the critical state for the MN and DP-MC in the axisymmetric extension is the same but not equal to the corresponding value for the axisymmetric compression. For both criteria, the mobilised friction at the critical state on the deviatoric plane decreases from the axisymmetric compression to the axisymmetric extension by increasing the Lode's angle (based on the definition in equation (19)). According to Fig. 1(b), since the MN smoothly circumscribes the DP-MC surface, it gives higher friction for the other loading directions than the axisymmetric loadings. However, as shown in the following, this is not generally the case for states other than the critical state.

To have a more effective visual impression of the friction mobilisations for different directions, several deviatoric cross-sections of the dynamic surfaces on both looser and denser sides of the critical state envelope are illustrated in Figs. 2 and 3.

Fig. 2 indicates that as the norm of the stress ratio increases, the Lode angle dependency (the directional effect of stress ratio) of the convex envelope of MN friction also increases. As shown, with the increase in the norm of stress ratio, the convex friction envelope on the deviatoric plane diverges from the isotropic friction envelope of the DP until finally, it smoothly circumvents the DP-MC friction envelope at the

critical state. In this regard, even stronger anisotropic friction mobilisation (higher degree of Lode angle dependency) can be seen for the denser side in Fig. 3. However, on the denser side where the bimodal behavioural feature is dominant (Barreto and O'Sullivan, 2012), as the norm of stress ratio increases and more stress-ratio induced anisotropy is intensified, the friction envelope of the MN moves inside the DP-MC envelope and approaches a triangular envelope with smoothly rounded edges. Indeed, the triangular shape is the maximum possible envelope in the Haigh-Westergaard stress space on which the principal stresses are greater than zero. Note that negative principal stresses are meaningless for a particulate material without any tensile capacity.

On the contrary, the DP and DP-MC criteria do not show this stress ratio-induced anisotropic faeture. In fact, the shape of DP and the DP-MC friction envelopes remain constant irrespective of the norm of stress ratio (being on the looser or denser side of the critical state envelope). The reason is that in both friction criteria, the dissipative shear mechanism ($\dot{\varepsilon}^p_{s,OCT}$) and the friction mobilisation (η_{OCT}) are established on the fixed octahedral plane. The only difference is that the DP-MC friction criterion is dependent solely on the direction of η via the shape function defined in the equation (18).

Prashant and Penumadu (2005a), after conducting a series of true triaxial tests on Kaolin clay, observed a similar anisotropic friction mobilisation on the looser and denser sides of the critical state envelope. Remarkably, they have reported a significant anisotropic behaviour on the denser side in terms of the deviatoric stress measure versus the deviatoric strain measure for the undrained true triaxial loadings under different Lode angles. Prashant and Penumadu (2005a) interpreted this anisotropic behaviour as an "inherent anisotropy" maintained in "the memory of soil" after the K_0-consolidation of the specimen in the preparation phase. These results, however, support the MN friction mobilisation (equation (14)) in which the anisotropic behaviour intensifies by moving from the critical state to the denser side, as shown in Fig. 3. This induced anisotropy could be linked to the bimodal stress transmission in DEM studies (e.g., Barreto and O'Sullivan (2012), Fleischmann (2020), Thornton (2000), Zhou et al. (2021)) although the
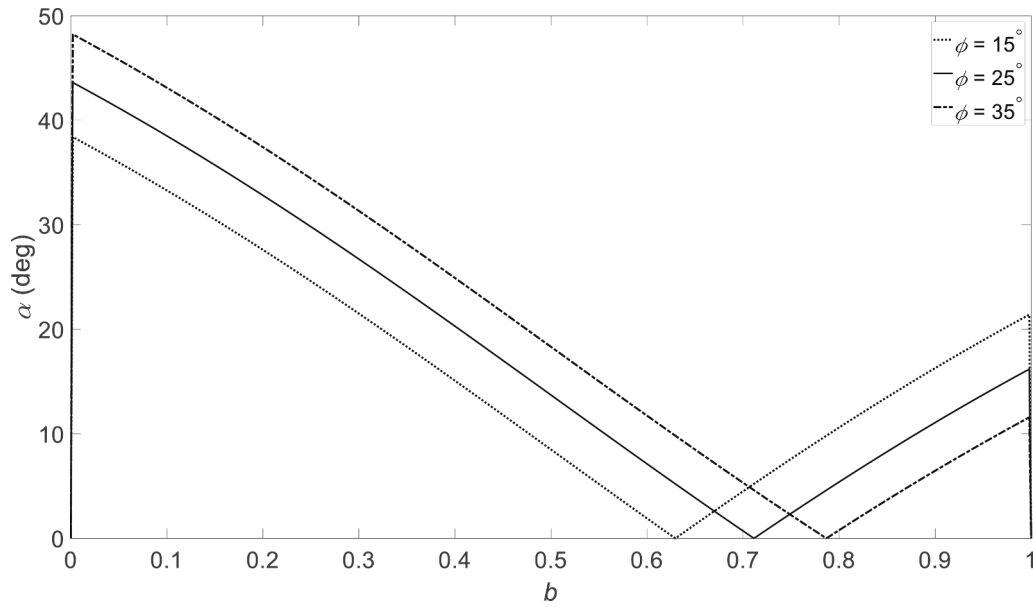
Fig. 5. Variation of the angle (α) between the inelastic flow vectors and the gradient of the surface in the deviatoric plane against the intermediate principal stress ratio (b) for the conventional Mohr-Coulomb (DP-MC) friction criterion, when $\varphi = 15°$, $25°$, and $35°$.

superiority of the experimentally developed Lade-Duncan friction envelope (Lade and Duncan, 1975) with greater friction in extension than the MN equivalent friction is acknowledged.

As a final remark, the notion of stress ratio-induced anisotropy in the MN friction criterion accommodated via equation (20) should certainly be distinguished from other types of friction or failure criteria (e.g. Gao et al. (2010)) with anisotropic features incorporated by the mixed invariant of the stress tensor and structure tensor (so-called fabric tensor).

6. Inelastic flow

The inelastic strain (the internal variable) can be computed from the differentiation of the flow potential with respect to the work-conjugated dissipative stress. Therefore, after invoking Ziegler's orthogonality postulate, i.e., $\chi = \sigma$, the inelastic strain rate related to friction criteria of the DP and the MN can be computed as equations (23) and (24) respectively:

$$\dot{\boldsymbol{\varepsilon}}^p = \frac{\partial w_{OCT}}{\partial \chi} = r \left(\frac{p_{eq}}{p_0}\right)^{\frac{1}{n-1}} \left(\left[1 - \left(\frac{\eta_{OCT}}{M_{OCT}}\right)^2\right]\left(\frac{1}{3}\right)\mathbf{1} + \left(\frac{3}{M_{OCT}^2}\right)\left(\frac{^D\boldsymbol{\sigma}}{p}\right)\right)$$

(23)

$$\dot{\boldsymbol{\varepsilon}}^p = \frac{\partial w_{SMP}}{\partial \chi}$$

$$= r\left(\frac{p_{eq}}{p_0}\right)^{\frac{1}{n-1}}\left(\left[1 - \left(\frac{\eta_{SMP}}{M_{SMP}}\right)^2\right]\left(\frac{1}{3}\right)\mathbf{1} - \left(\frac{2}{M_{SMP}^2}\right)\left(p \quad {}^D(\boldsymbol{\sigma}^{-1})\right)\right)$$

(24)

The inelastic strain rate for the case with the DP-MC friction criterion is the same as equation (23), but with the value defined in equation (18) instead of M_{OCT}. As equations (23) and (24) indicate, the inelastic strain increment and the current stress are coaxial for all cases. This can be acknowledged as one of the limitations of the model since real and virtual experiments (e.g. Roscoe (1970), Gutierrez and Ishihara (2000), Pouragha et al. (2021), and Karapiperis et al. (2020)) on frictional particulate material have demonstrated the non-coaxiality between the current stress and inelastic flow.

It is essential to recognise that the dissipative and true stresses have different natures, although they are equal due to the absence of plastic free energy based on Ziegler's orthogonality postulate. As its name

indicates, χ has a dissipative nature, whilst σ has a conservative nature. This difference allows the introduction of non-associated inelastic flows whose directions are not perpendicular to the dynamic surface in the true stress space. The non-associativity of inelastic flow could be considered by elastoplastic coupling in the conservative or dissipative forms (Collins, 2002). The current paper only considers the dissipative coupling, based on which the dissipation function is coupled with the current true stress state. According to the flow potential (equation (16)), due to the lack of dissipative coupling, the inelastic flow for the DP friction criterion defined in equation (23) is associated.

On the other hand, the flow potential for the DP-MC friction criterion (equation (16) with replacement of M_{OCT} by equation (18)) is dependent on the stress ratio but only on its direction (via equation (19)), leading to the non-associated inelastic flow. Fig. 4 illustrates the inelastic flow directions (depicted by arrows) for this case on the p-q and the deviatoric planes at the critical state ($\text{tr}(\dot{\boldsymbol{\varepsilon}}^p) = 0$). As shown in Fig. 4(a), the inelastic flow direction on the p-q plane is associated regardless of the value of φ. However, following the directional dependency of the force and the flow potentials on the current η through equations (18) and (19), the inelastic flow is non-associated, exclusively on the deviatoric plane.

Another interesting observation is the variation of the degree of non-associativity of in-elastic flow with φ. The degree of non-associativity (α) is defined as the angle between two vectors of the inelastic flow and the gradient of the dynamic surfaces on the deviatoric plane. Fig. 5 shows the degree of non-associativity (α) for the DP-MC friction against the intermediate principal stress ratio (b):

$$b = \frac{\sigma_2 - \sigma_3}{\sigma_1 - \sigma_3} = \frac{\sqrt{3}\tan(\theta) + 1}{2}$$

(25)

As shown in Fig. 5, for the more significant part of the DP-MC friction envelope, α increases with the increase of φ. Note that there is a sharp change in the degree of non-associativity in the vicinity of the axisymmetric condition ($b = 0, 1$). However, the dependency of α on the value of φ is not due to the change of inelastic flow direction with the change of φ. As shown in Fig. 4b, for a certain direction of η (or Lode angle), the inelastic flow direction of the DP-MC friction is constant and the same as the DP inelastic flow. It is the anisotropic evolution of the DP-MC friction mobilisation with an increase of φ, and subsequently, the evolution of the gradient vector of the DP-MC hexagon that indeed causes the change of α. This kind of inelastic flow has been reported by Prashant and
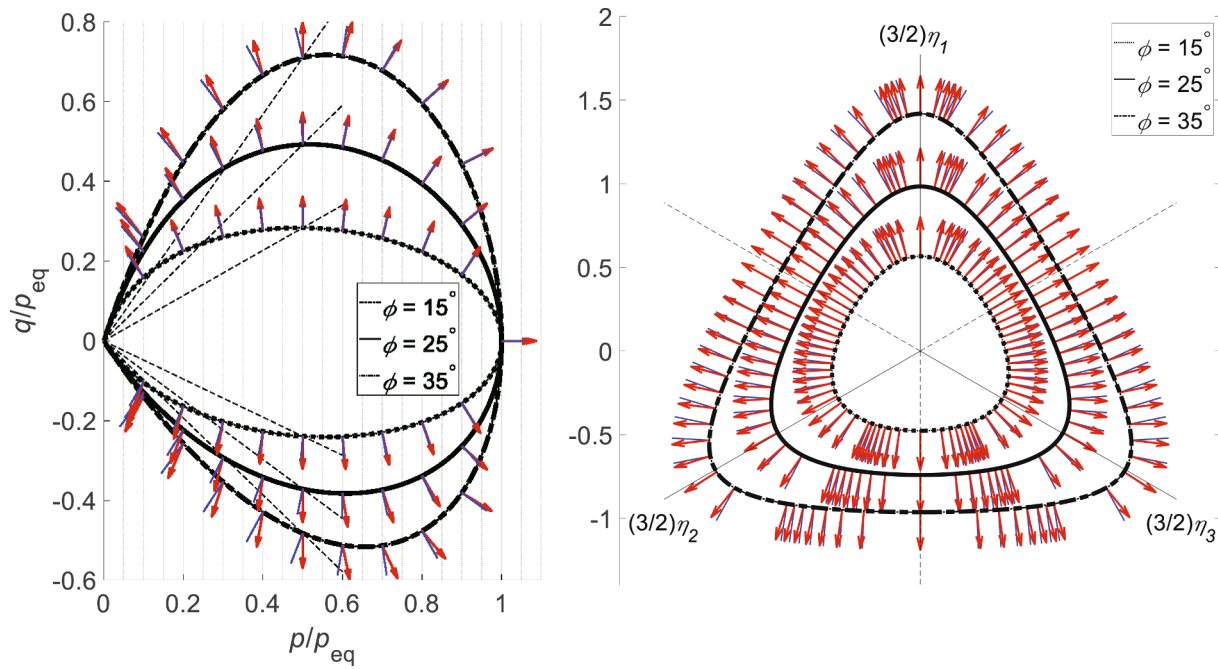
Fig. 6. Dynamic surfaces and the corresponding inelastic flow directions on (a) the normalised meridian plane (b) the deviatoric plane at the critical state for the Matsuoka-Nakai (MN) friction criterion when $\varphi = 15°$, $25°$, and $35°$- Note that the vectors without arrows next to each inelastic flow vectors are the gradient of the deviatoric surface. Moreover, the left side scale in (b) is a metric for the stress ratio (representative of friction) at the critical state in one out of three possible situations for axisymmetric compression.
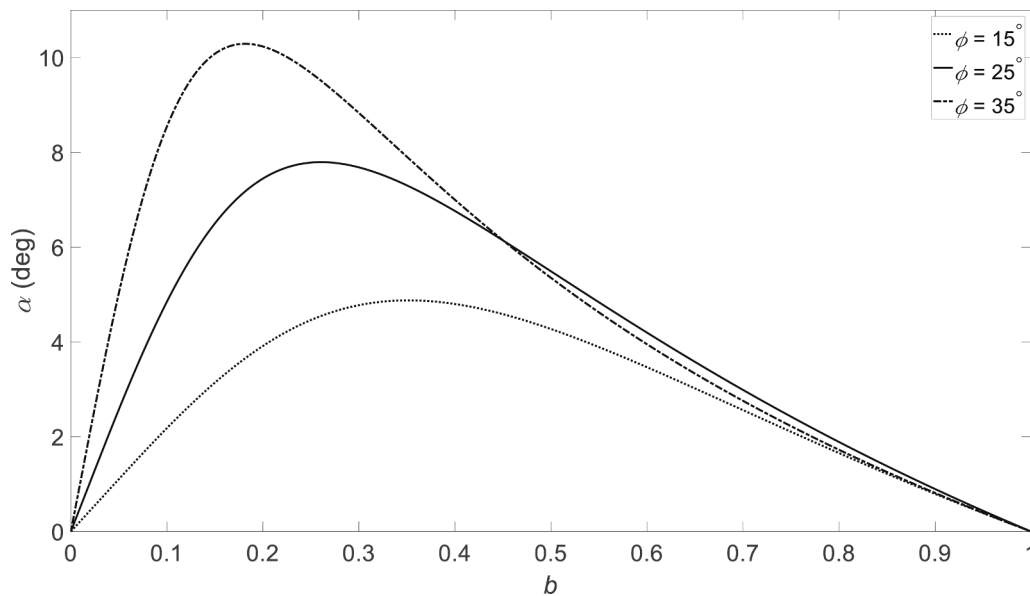
Fig. 7. Variation of the angle (α) between the inelastic flow vectors and the gradient of the surface in the deviatoric plane against the intermediate principal stress ratio (b) for the Matsuoka-Nakai (MN) friction criterion, when $\varphi = 15°$, $25°$, and $35°$.

Penumadu (2004) and Prashant and Penumadu (2005b) for kaolin clay, and it has been employed in solving some boundary value problems (e.g. Potts and Gens (1984), Grammatikopoulou et al. (2007) and Shirmohammadi et al. (2021)).

The inelastic flow direction for the MN friction criterion in the triaxial stress plane and the deviatoric plane at the critical state is illustrated in Fig. 6. Contrary to the DP and DP-MC friction criteria, the inelastic flow is non-associated in both the triaxial and the deviatoric plane as the dissipative mechanism depends on both the direction and norm of η. In solid materials like metal, the magnitude of the yielding deviatoric stress governs the dissipation and inelastic flow. In

particulate frictional materials, both the norm and direction of the stress ratio control the dissipation and inelastic flow, which is the case for the MN dissipation mechanism (equation (20)). This view criticises the dissipative mechanism considered for the DP and the DP-MC to be a frictional type.

As shown in Fig. 6, the degree of non-associativity in both stress planes increases with an increase in φ. On the triaxial plane, a "stress softening" behaviour on the looser side in the vicinity of the critical state in both extension and compression emerges for large values of φ. However, the inelastic volumetric flow in these regions is still contractant, consistent with the CSSM.
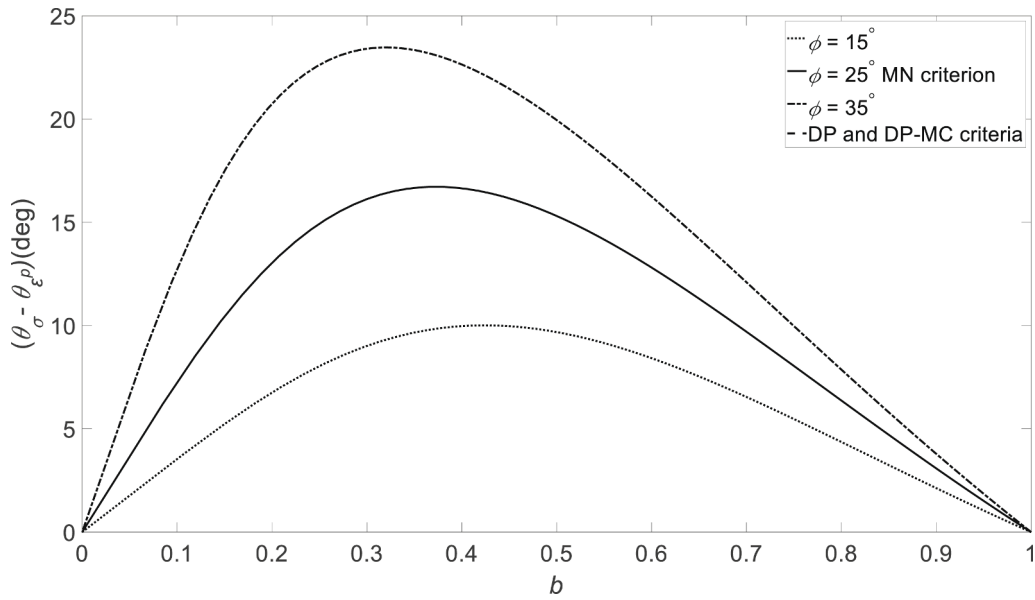
Fig. 8. Comparison of the deviations (disaccord) between the stress Lode angle (θ_σ) and the inelastic strain Lode angle (θ_{ε^p}) in the Drucker-Prager (DP), the conventional Mohr-Coulomb (DP-MC), and the Matsuoka-Nakai (MN) friction criteria when $\varphi = 15°$, $25°$, and $35°$.
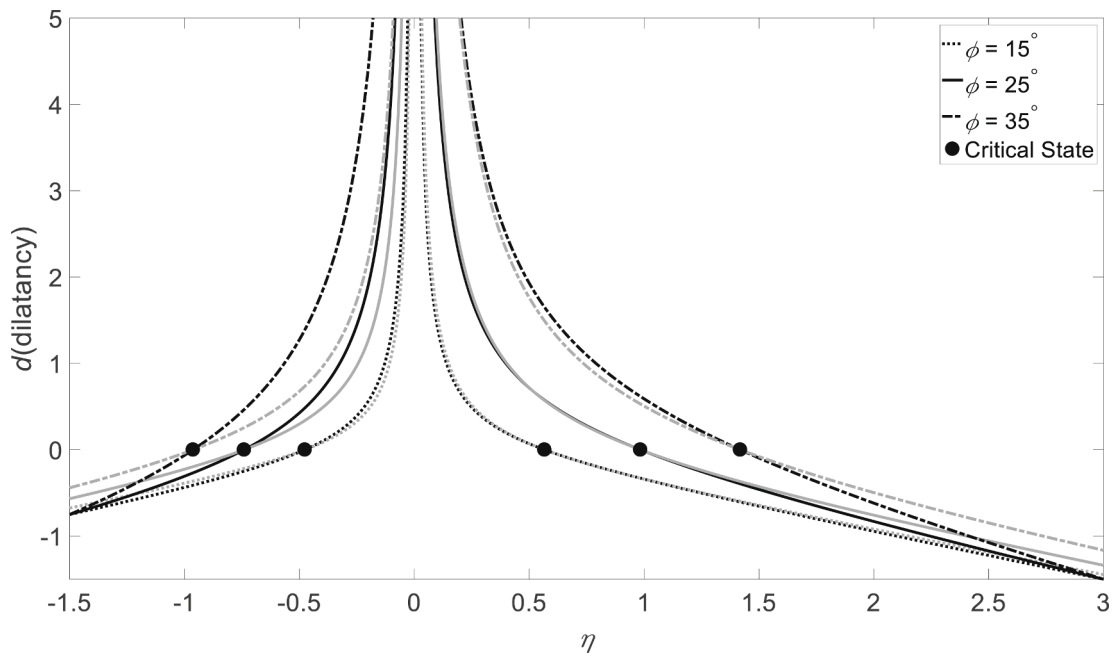

Fig. 9. Comparison of the dilatancy under axisymmetric condition for the conventional Mohr-Coulomb (DP-MC) and the Matsuoka-Nakai (MN) friction criteria when $\varphi = 15°$, $25°$, and $35°$.

Fig. 7 shows the pattern of increase in the degree of non-associativity (α) in the deviatoric plane for the MN friction criterion. In contrast to the DP-MC criterion, the relative position of the inelastic flow to the gradient of the MN convex surface does not change and always remains on one side of the gradient vectors.

According to Fig. 6 (b), the inelastic flow and the current stress state in the deviatoric plane for the MN friction criterion are not in the same direction. This feature has been observed in several experimental studies, e.g. Yong and McKyes (1971), Lade and Musante (1978), Nakai et al. (1986), Topolnicki et al. (1990), and Kirkgard and Lade (1993).

Fig. 8 shows the relationship between the direction of the inelastic flow and the stress ratio on the deviatoric plane in terms of the difference between their Lode angles (discordance) at a particular stress state.

For the computation of θ_{ε^p}, equation (19) with the definition of $\eta_{\varepsilon^p} = {}^D\dot{\varepsilon}^p / \sqrt{tr^2(\dot{\varepsilon}^p)}$ instead of η is employed. Since the inelastic flow in the DP-MC and DP friction criteria is perpendicular to a circular potential on the deviatoric plane, there is no discordance between the Lode angles associated with the stress state and its corresponding inelastic flow vector. However, for the MN friction criteria, except for the axisymmetric stress states ($b = 0$, 1), the disaccord is intensified by an increase in the value φ. This observation is consistent with DEM studies of Zhou et al. (2021), Thornton and Zhang (2010), Wan and Pinheiro (2014), and Karapiperis et al. (2020), in addition to the aforementioned experimental studies.

Finally, but importantly, the inelastic dilatancy (d), the ratio of the volumetric and the norm of the deviatoric component of the inelastic
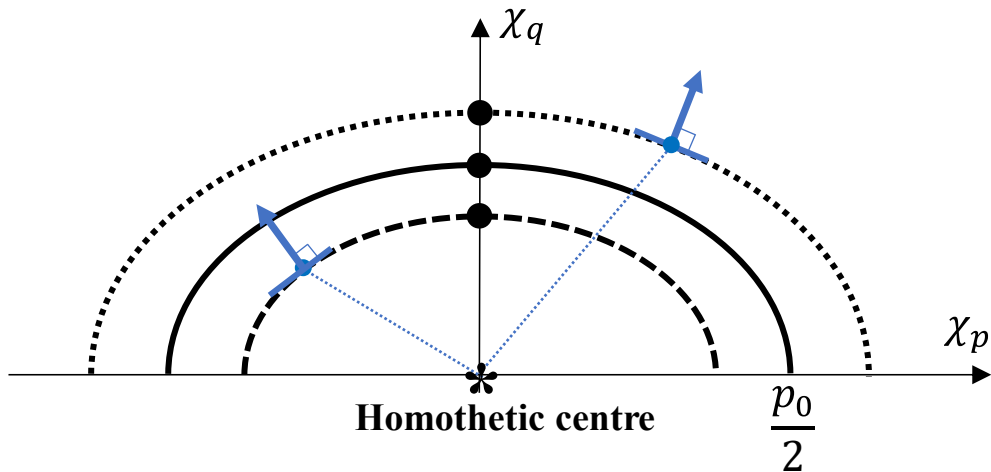
Fig. 10. Viscous homotheticity and the critical states associated with different loading rates in the dissipative stress space.

strain increment under axisymmetric condition, for the DP-MC and MN friction criteria are compared in Fig. 9. The dilatancy for the cases with DP-MC and MN friction criteria are computed from equations (23) and (24) respectively, and they are presented against the triaxial stress ratio η. The negative and positive sides of η represent the axisymmetric extension and compression. As shown, by increasing φ, the dilatancy of the MN friction criterion gets larger than the equivalent dilatancy for the DP-MC criterion, particularly for the axisymmetric extension. However, the critical state (zero dilatancy) associated with each value of φ is unique for both criteria, consistent with the previous observations.

Fig. 9 also shows that the dilatancy of the MN criterion approaches the unique values of -1.5 and -0.75 for the axisymmetric compression and extension as the stress ratio approaches $\eta = 3.0$ and $\eta = -1.5$ representing the tension cut-off lines for the axisymmetric compression and axisymmetric extension, respectively.

7. Possible Ill-Formulations causing Non-Uniqueness of friction at the critical state

Houlsby (1981) presented the hyperplastic description of the rate independent MCC model in which the volumetric plastic work has been divided into the stored (integrable) and dissipative shares. Alternately, Collins and Houlsby (1997a) and Houlsby (2000) presented another hyperplastic form of the MCC model in which the entire plastic volumetric work has been placed in the non-negative definite dissipation function. The non-unique expression of the MCC model brought Houlsby (2000) to the conclusion that free energy and dissipation are generally unobservable.

On the other hand, Collins and Hilder (2002) proposed a family of critical state models with versatile yield surfaces and non-associated inelastic flow rules for a rate-independent system with a single internal variable. In these models, by imposing Ziegler's orthogonality postulate, the location of the critical state on the spherical stress axis is adjustable (adjustable spacing ratio) due to the adjustability of the dissipative and stored shares of the plastic volumetric work while the critical state friction envelope remains unique. Considering these distinctions, it is tempting to employ the same forms of potentials proposed by Collins and Hilder (2002) to construct a family of the critical state model for an equivalent rate-dependent system (e.g. Jacquey and Regenauer-Lieb (2021)). However, Grimstad et al. (2020) and Grimstad et al. (2021) demonstrated that this comes at the expensive cost of losing the unique critical state friction envelope under different loading rates in hyper-viscoplastic models with homothetic viscosity. Two sources for

this non-uniqueness are specified in the following.

To reveal the first source, suppose the following form for the force potential:

$$z = \left(\frac{rp_0}{n}\right)\left(\frac{\sqrt{\text{tr}^2(\dot{\boldsymbol{\varepsilon}}^{\mathbf{p}}) + (\overline{\mathbf{M}}\dot{\bar{\varepsilon}}_{\mathbf{s}}^{\mathbf{p}})^2}}{2r}\right)^n \tag{26}$$

This form of the force potential with the same parameters as in equation (5) is similar to the MCC dissipation function (Houlsby, 1981). The only differences are the homogeneity order n resulting in the homothetic scaling relation for viscosity (with respect to reference strain rate r), whose centre is located at the origin of the dissipative space. This is illustrated schematically in Fig. 10, with the vectors representing the direction of the inelastic flow in the dissipative stress space. As shown, the critical states (represented by bullets) associated with different loading rates are located on χ_{q} axis ($\chi_{\mathrm{p}} = 0$) along with the homothetic centre.

The last modification to obtain a hyper-viscoplastic model with a similar form to the hyperplastic MCC model of Collins and Hilder (2002) is the addition of a volumetric plastic part to the free energy potential expressed in equation (2):

$$f = \kappa p_a \exp\left(\frac{\text{tr}(\boldsymbol{\varepsilon} - \boldsymbol{\varepsilon}^{\mathbf{p}}) + \text{gtr}\left(\left(^{\mathrm{D}}\boldsymbol{\varepsilon} - {}^{\mathrm{D}}\boldsymbol{\varepsilon}^{\mathbf{p}}\right)^2\right)}{\kappa}\right) + \left(\frac{\lambda - \kappa}{2}\right)\underbrace{p_{\mathrm{ref}}\exp\left(\frac{\text{tr}(\boldsymbol{\varepsilon}^{\mathbf{p}})}{\lambda - \kappa}\right)}_{p_0} \tag{27}$$

where p_0 is the CSSM hardening variable employed in the dissipation function (equation (26)) as well. Based on the hyperplastic framework, the outcome of having a plastic part in the free energy is a shift or back stress which is employed in transforming the dissipative stress space to the true stress space by invoking Ziegler's orthogonality postulate (Collins and Houlsby, 1997a; Houlsby and Puzrin, 2007). The shift stress here is equal to $p_0/2$ computed by derivation of the plastic part of free energy with respect to the volumetric inelastic strain. The shift stress essentially has a non-viscous nature since it cannot bear any viscous homothetic scaling in terms of the rate of the internal variable. This is due to the nature of the free energy function that describes the path-independent behaviour of a system.

Fig. 11 illustrate the effect of non-viscous shift stress on the dynamic surface with the DP-MC and MN friction criteria in the true stress space. As shown, the homothetic centre in both cases has been moved to the non-viscous shift stress after imposing Ziegler's orthogonality postulate
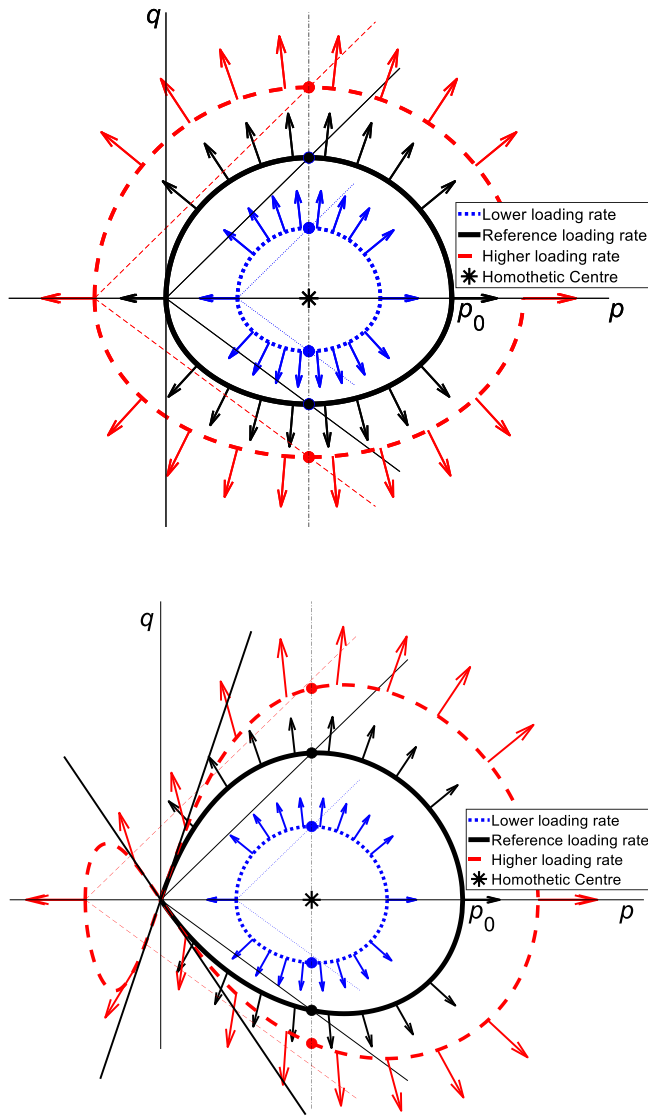
Fig. 11. Dynamic surfaces together with inelastic flow direction in the true stress space for (a) the conventional Mohr-Coulomb (DP-MC) and (b) Matsuoka-Nakai (MN) friction criteria showing the non-uniqueness of the critical state friction under different loading rates due to movement of the homothetic centre as the consequence of consideration of plastic free energy for the rate-dependent system with a single internal variable.

($\chi_p = p - p_0/2$). The inelastic flow directions corresponding to the different loading rates are also depicted in the figure. Also shown are the critical states (bullet points) on the axis $p = p_0/2$, each associated with different loading rates. This indicates that the mobilised friction at the critical state ($tr(\dot{\boldsymbol{\varepsilon}}^p) = 0$) could generally attain any value depending on the loading rate history. The effect of the tension cut-off on the mobilised friction in the MN criteria can also be observed in Fig. 11(b). Compared with the DP-MC friction criterion, the dynamic surface with the MN criterion is twisted around tension cut-off lines.

Discard of the plastic free energy may not necessarily guarantee a unique critical state friction envelope for rate dependency if the force potential (dissipation function) is coupled with the internal variable in such a way that it affects the homothetic viscosity. To expose this second

source, $\overline{M}$ in the force potential defined in equation (5) is modified into the following form similar to the one proposed by Collins and Kelly (2002):

$$\overline{M} = M_{SMP}\left[1 - \gamma + \gamma\left(\frac{2p}{p_0}\right)\right] \tag{28}$$

in which p_0, as defined in equation (6), is a function of the volumetric component of the internal variable. Equation (28) incorporates the spherical effective stress dependency of shear dissipation (an essential attribute of frictional material) by mapping M_{SMP} based on the ratio of p/p_0 to secure a correct dimension for the dissipation rate.

By following the same procedure as before, the dynamic surface in the dissipative stress space with the modified $\overline{M}$ can be computed similarly to equation (13):

$$p_{eq} = \chi_p\left[1 + \left(\frac{\sqrt{ptr(\boldsymbol{\sigma}^{-1}\cdot(\,^D\boldsymbol{\chi})^2)}}{\overline{M}\chi_p}\right)^2\right] \tag{29}$$

After applying Ziegler's orthogonality for this case ($\boldsymbol{\chi} = \boldsymbol{\sigma}$), a similar dynamic surface to equation (14) but with the new friction coefficient (equation (28)) can be obtained:

$$p_{eq} = p\left[1 + \left(\frac{\eta_{SMP}}{\overline{M}}\right)^2\right] \tag{30}$$

The dynamic surface associated with different loading rates and the corresponding inelastic flow direction for the fascinating situation of $\gamma = 1$ are illustrated in Fig. 12. As shown, the paradigm of the CSSM is lost for different loading rates due to the loss of the homothetic viscosity caused by the mapping of frictional coefficient based on a non-viscous hardening variable (p_0). Grimstad et al. (2021) have utilised this later condition to propose a relation for the evolution of the earth pressure coefficient at rest due to creep.

It is also notable that the dynamic surfaces become concave in their dilatant part, equivalent to the rate-independent case (Collins and Kelly, 2002). Although this non-convexity violates Drucker's stability postulate (Drucker, 1959), it is not an issue from both aspects of thermodynamics and the rheology of the material. Since the dissipative stress is equal to the true stress in the absence of the plastic free energy, it is evident from Fig. 12 that the dissipation is non-negative definite and maximal (see Appendix D), even in the concave region. Moreover, increasing the loading rate, which is envisaged by the increase of the size of dynamic surfaces, results in a higher stress state for the material, which is rheologically sensible.

8. A set of hyper-viscoplastic critical state models

To generate a broad set of hyper-viscoplastic critical state models with versatile dynamics surface and the flow rule while simultaneously securing a unique critical friction envelope, Dadras-Ajirloo et al. (2022) proposed the following form for the force potential:

$$z = \frac{rp_0}{n}\left(\frac{\sqrt{tr^2(\overline{\mathbf{T}}\dot{\boldsymbol{\varepsilon}}^{\mathbf{p}}) + (\overline{M}\dot{\boldsymbol{\varepsilon}}^{\mathbf{p}}_{\mathbf{s}})^2} + tr(\dot{\boldsymbol{\varepsilon}}^{\mathbf{p}})}{Rr}\right)^n \tag{31}$$

where R is called the spacing ratio, specifying the relative location of the critical state on the spherical stress axis for dynamic surfaces. Chen and Yang (2017) have reported that the spacing ratio for clays can vary between 1.5 and 4.0. While Dadras-Ajirloo et al. (2022) presented the force potential (equation (31)) for the DP criterion, here it is generalized
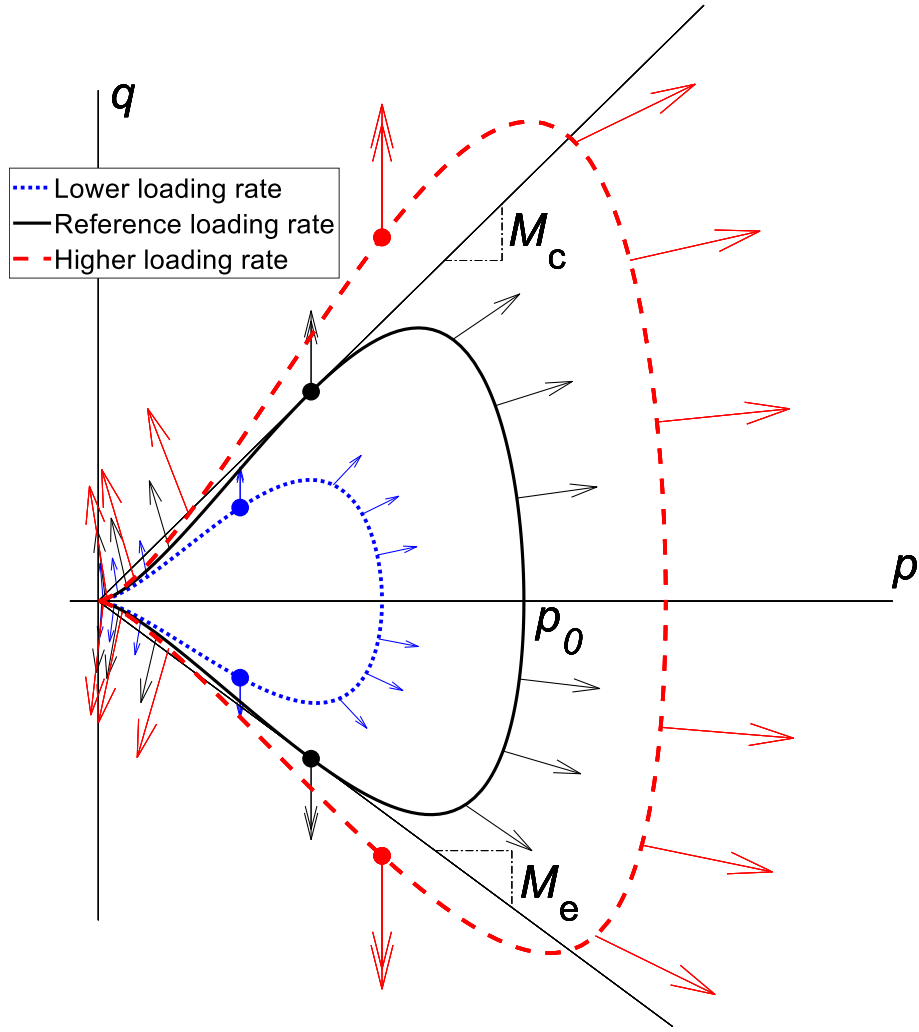
Fig. 12. Dynamic surfaces together with inelastic flow direction in the true stress space for Matsuoka-Nakai (MN) friction criteria showing the non-uniqueness of the critical state friction under different loading rates due to the non-homotheticity of the viscous scaling as the consequence of mapping of frictional coefficient in equation (32).

to other friction criteria by a consistent specification of $\overline{T}$, $\overline{\dot{\varepsilon}}^p_s$, and $\overline{M}$ for the intended frictional criterion. The dimensionless coefficient $\overline{T}$ is a variant of the Logistic function, which due to its performance called the transition function of the state variable $\overline{S}$, defined as:

$$\overline{T} = \frac{R}{2} + \left(\frac{R}{2} - 1\right)\tanh(\overline{S}) \tag{32}$$

chosen friction criterion. For $R = 2$ and subsequently $\overline{T} = 1$, the classical force potential expressed in equation (5) can be retrieved. By following the procedure as previously, the flow potential with the same form as equation (8) can be computed in which the general equivalent isotropic stress measure (p_{eq}) in the dissipative stress space is:

$$p_{eq} = \frac{R\chi_p \sqrt{\left(\left(\chi_p\overline{M}\right)^2 - \overline{\chi}_q^2\right)^2 + \overline{\chi}_q^2\left(\chi_p\overline{MT} + \sqrt{\left(\chi_p\overline{M}\right)^2 + \left(\overline{T}^2 - 1\right)\overline{\chi}_q^2}\right)^2}}{\overline{T}\left(\left(\chi_p\overline{M}\right)^2 - \overline{\chi}_q^2\right) + \sqrt{\left(\left(\chi_p\overline{M}\right)^2 - \overline{\chi}_q^2\right)^2 + \overline{\chi}_q^2\left(\chi_p\overline{MT} + \sqrt{\left(\chi_p\overline{M}\right)^2 + \left(\overline{T}^2 - 1\right)\overline{\chi}_q^2}\right)^2}} \tag{34}$$

$$\overline{S} = \left(\frac{\overline{M}}{\overline{\eta}}\right)^2 - \left(\frac{\overline{\eta}}{\overline{M}}\right)^2 \tag{33}$$

in which the critical state friction is treated as a reference according to the CSSM. The detailed description of $\overline{M}$ and $\overline{\eta}$ depend on the

By specialising the generalised force potential for the MN friction criterion by assuming $\overline{\dot{\varepsilon}}^p_s = \sqrt{3}\dot{\varepsilon}^p_{s,DKP}$, $\overline{M} = M_{SMP}$, and $\overline{\eta} = \eta_{SMP}$, the components of dissipative stress $\left(\chi_p, \overline{\chi}_q\right)$ in equation (34) are computed to be the same as their corresponding values previously computed for the classical force potential. Since there is no plastic free energy and
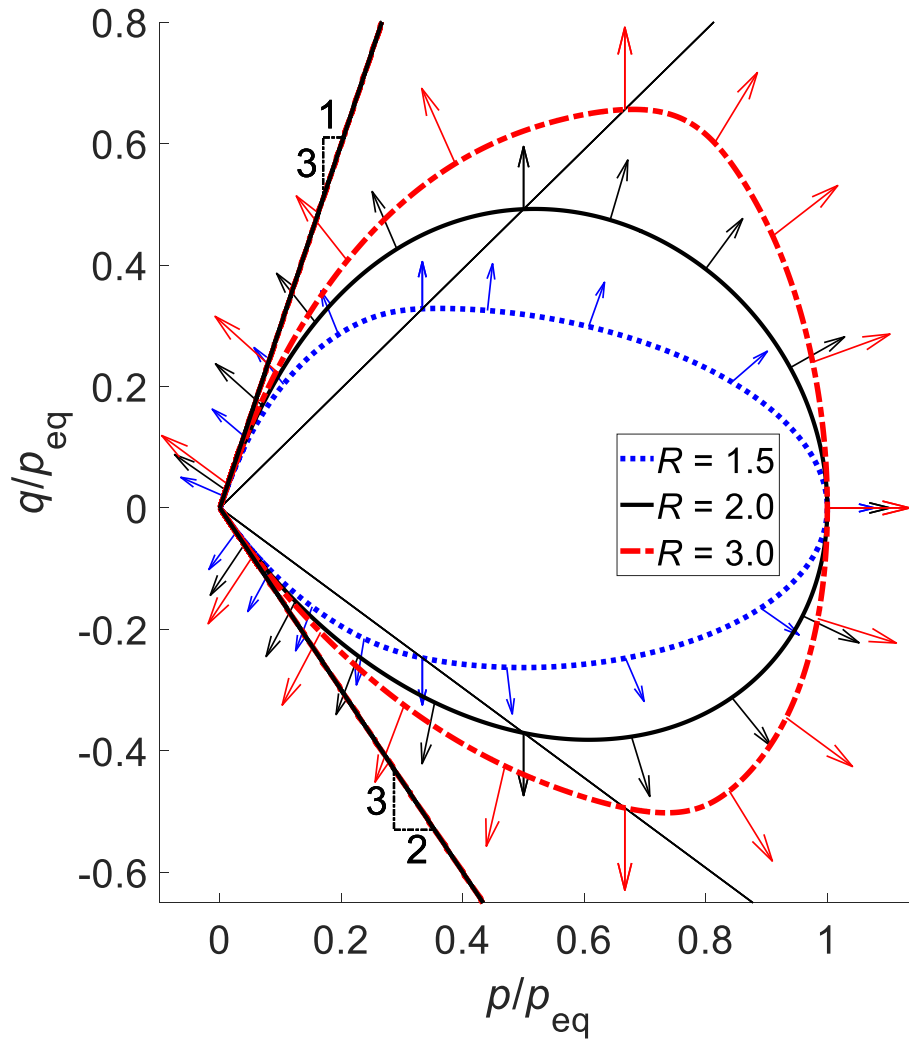
Fig. 13. The convex dynamic surface hybridised with the Matsuoka-Nakai (MN) friction criteria together with the corresponding inelastic flow directions (arrows) in the normalised true stress space for different values of spacing ratio (R) and $\varphi = 25°$.

subsequently no shift stress, invoking Ziegler orthogonality condition ($\chi = \sigma$) yields the following expression for p_{eq} in the true stress space:

$$p_{eq} = \frac{Rp\sqrt{\left(M_{SMP}^2 - \eta_{SMP}^2\right)^2 + \eta_{SMP}^2\left(TM_{SMP} + \sqrt{M_{SMP}^2 + (T^2-1)\eta_{SMP}^2}\right)^2}}{T\left(M_{SMP}^2 - \eta_{SMP}^2\right) + \sqrt{\left(M_{SMP}^2 - \eta_{SMP}^2\right)^2 + \eta_{SMP}^2\left(TM_{SMP} + \sqrt{M_{SMP}^2 + (T^2-1)\eta_{SMP}^2}\right)^2}} \tag{35}$$

Fig. 13 illustrates the effect of the spacing ratio parameter on the convex loci and their corresponding inelastic flow. As shown, the dilatancy is controlled by the ratio of the mobilised friction to the critical friction and the spacing ratio. This is the fundamental premise of the CSSM employed through the sophisticated and comprehensive force potential defined in equation (31) which guarantees the uniqueness of the critical friction envelope.

It is still possible to increase the versatility of the force potential by incorporating the "frictional dissipation", i.e., the spherical effective stress sensitivity of a dissipative shearing process attributed to the mobilisation of internal friction at grains/aggregates contacts. To do so,

by preserving the dimension of the force potential, $\overline{M}$ in equation (31) can be modified to:

$$\overline{M} = M_{SMP}\sqrt{1 - \gamma + \gamma\left(\frac{Rp}{\overline{p}_0}\right)} \tag{36}$$

It is important to note that $\overline{M}$ in the definition of the state variable S (equation (33)) is the critical state friction (for instance, $\overline{M} = M_{SMP}$ while $\overline{\eta} = \eta_{SMP}$ for the MN criterion), which following the CSSM serves as a reference, and is not affected by equation (36). Compared to equation (28) that led to the non-unique critical state friction envelope, there are three differences in equation (36). Firstly, after Zhang et al. (2018), the square root function is employed to have the convexity for the dynamic surface and more flexibility in adjusting the value of γ, which regulates
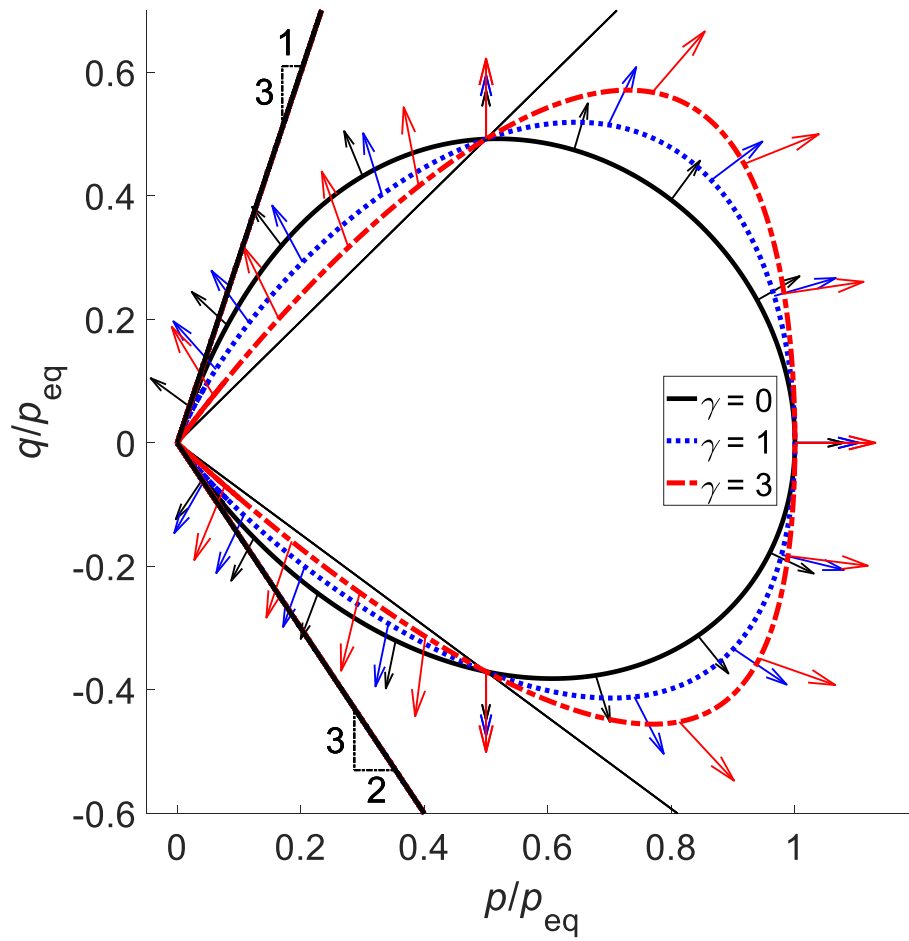
Fig. 14. The convex dynamic surface hybridised with the Matsuoka-Nakai (MN) friction criteria together with the corresponding inelastic flow directions (arrows) in the normalised true stress space for different values of parameter γ incorporating the frictional dissipation while $\varphi = 25°$ and $R = 2$.

the intensity of the spherical effective stress dependency of the shear dissipation. Secondly, parameter R is incorporated to secure the critical state friction at the desired spacing ratio. Lastly, instead of the non-

with the same form as equation (35) is recruited to preserve the homothetic viscosity and subsequently maintain a unique critical friction envelope. Therefore, equation (36) can be written as:

$$\overline{M} = M_{SMP}\sqrt{1 + \gamma\left(\frac{T\left(M_{SMP}^2 - \eta_{SMP}^2\right)}{\sqrt{\left(M_{SMP}^2 - \eta_{SMP}^2\right)^2 + \eta_{SMP}^2\left(TM_{SMP} + \sqrt{M_{SMP}^2 + (T^2-1)\eta_{SMP}^2}\right)^2}}\right)} \tag{37}$$

viscous hardening parameter p_0, the equivalent dynamic pressure $\overline{p}_0$

According to equations (36) and (37), the spherical effective stress sensitivity of the shear dissipation is linked to the relative value of the mobilised friction from the critical friction. Fig. 14 illustrates the effect of the frictional dissipation on the dynamic convex loci and their corresponding inelastic flow directions. As shown, with the increase of γ, the convex loci get more teardrop shapes while conforming to the tension cut-off due to the engagement of the MN friction. Moreover, incorporating the frictional dissipation mitigates the dilation on the denser side of the critical state. In contrast, it causes an increase in the contraction (negative dilatancy) on the looser side.

Table 1
Parameters of the model and their values for HKMD and Fujunomori clay.

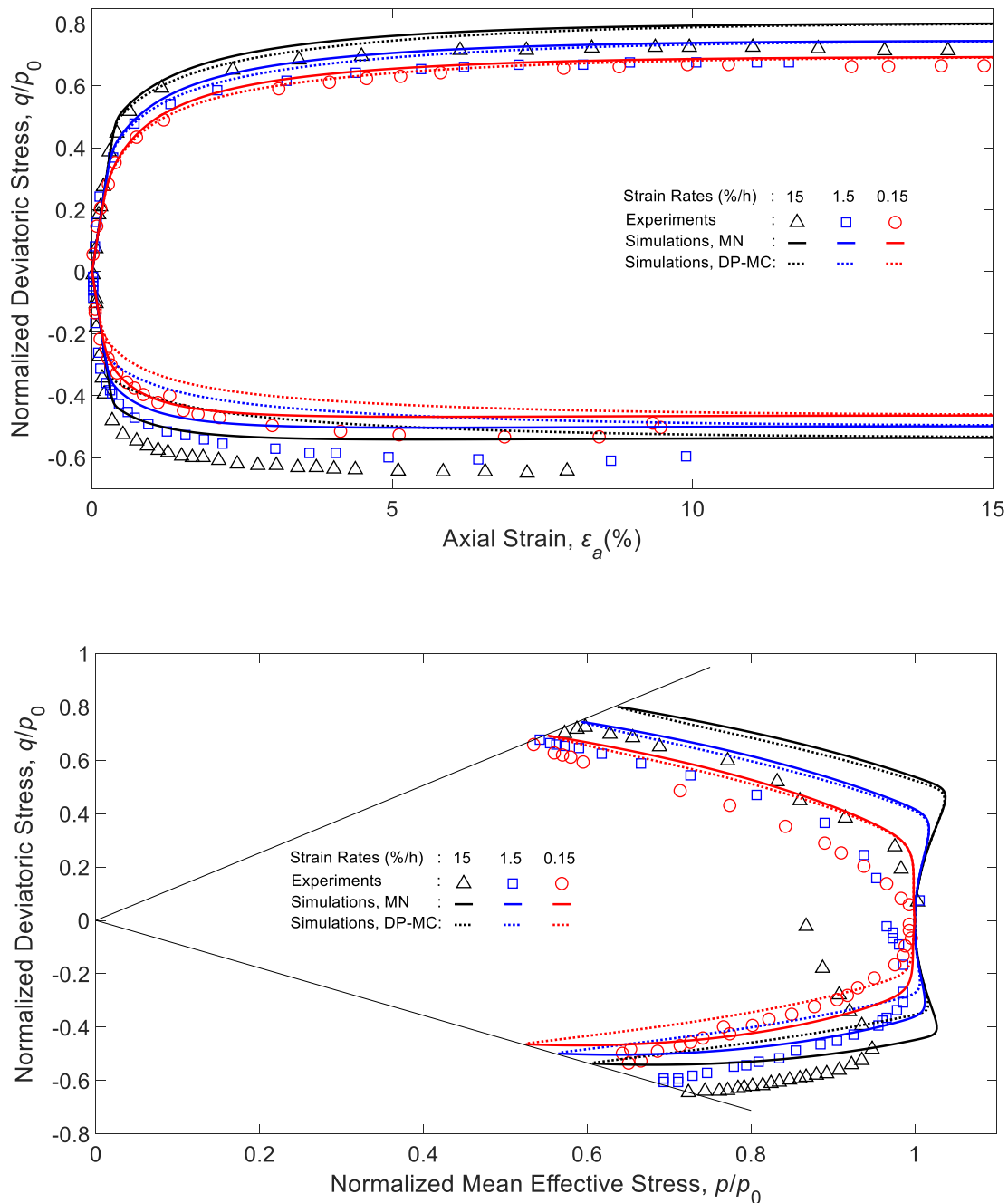| Model parameters	Description	HKMD	Fujinomori clay
κ	slope of isotropic unloading line on bi-logarithmic compression plane	0.018	0.0112
λ	slope of normal compression line on bi-logarithmic compression plane	0.0793	0.0508
g	shear modulus coefficient	42	88.2
φ	angle of shearing resistance at critical state	31.5°	33.7°
R	spacing ratio	2.6	2.2
γ	parameter for frictional dissipation	0	0
μ	creep index	0.0025	0.003

Fig. 15. Comparison between experimental and simulated results of undrained triaxial tests on normally consolidated reconstituted HKMD under different strain rates in terms of (a) stress–strain behaviour and (b) stress path.

9. Model evaluation

The efficacy of the developed hyper-viscoplastic model with DP-MC and MN friction criteria is evaluated by simulating the conventional and true triaxial test conducted on the Hong Kong Marine Deposits (HKMD) (Yin and Zhu, 1999, Zhu, 2000) and Fujinomori clay (Nakai and Matsuoka, 1986, Nakai et al., 1986). The model requires seven dimensionless parameters same as the previous version (Dadras-Ajirloo et al., 2022). Table 1 displays the model parameters and their values for both clays based on the report of the original experimental studies.

The only parameter not included in Table 1 but implicitly considered in the model is the reference strain rate, *r*. By definition, *r* is the average volumetric strain rate for a certain consolidation mode. It can be estimated from conventional 24-hour incremental loading oedometer or isotropic consolidation tests. This means that the stress–strain behaviour obtained from either of these two conventional tests can be taken as the reference stress–strain behaviour for the isotache viscous scaling considered in the force potential (equation (5)). For instance, for the oedometer test, the oedometer plastic strain rate under K_0 loading can be computed from the model as:

$$\dot{\varepsilon}_v^p\Big|_{oed} = 3\frac{\partial w}{\partial(tr(\chi))} = 3r\left(\frac{p_{eq}}{p_0}\right)^{\frac{\mu}{\lambda-\kappa}}\frac{\partial p_{eq}}{\partial(tr(\chi))}\Big|_{K_0} \tag{38}$$

in which equation (7) is replaced for *n*. Since the isotache associated with the K_0 loading is chosen as the reference, then $p_{eq} = p_0$, and:
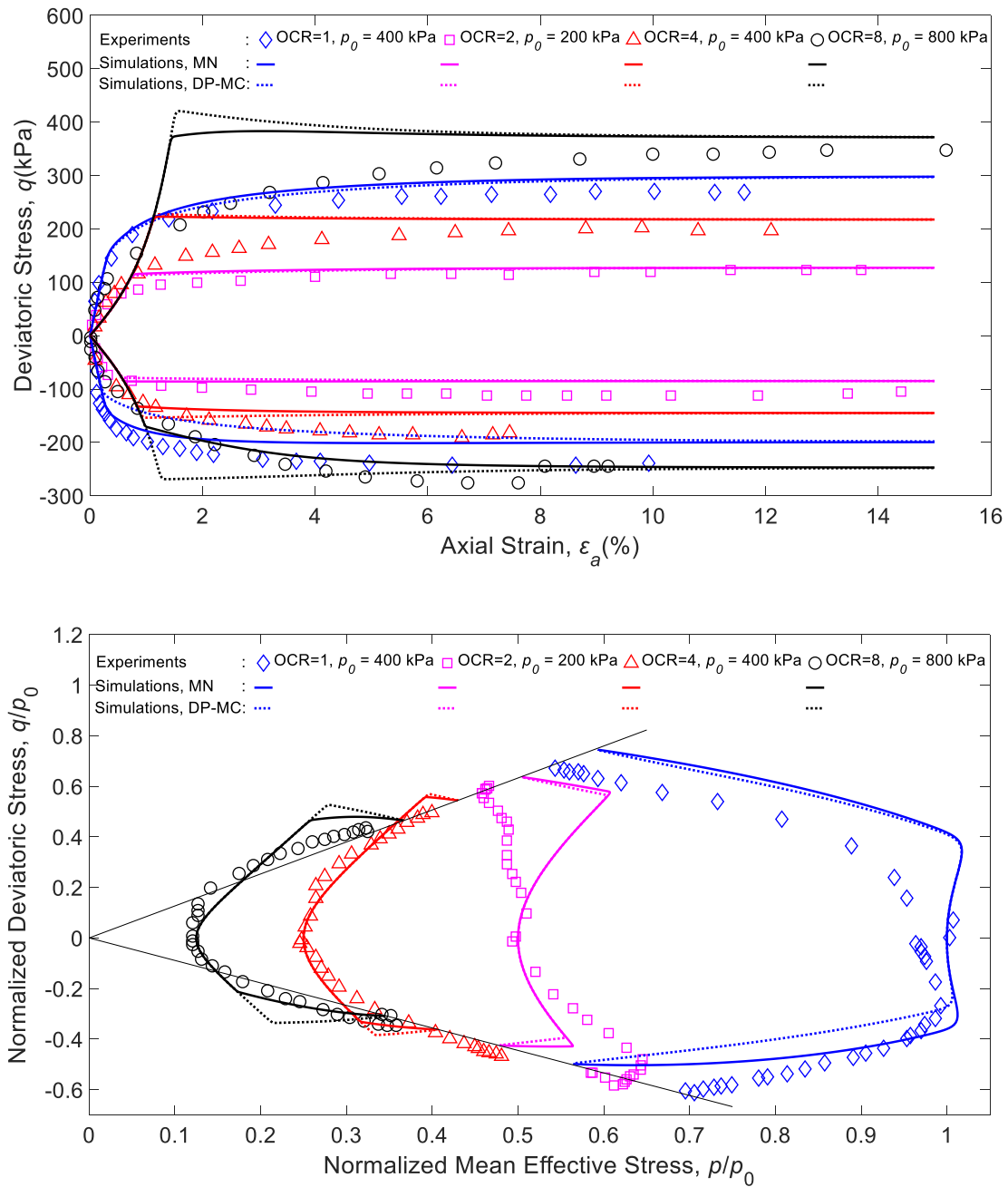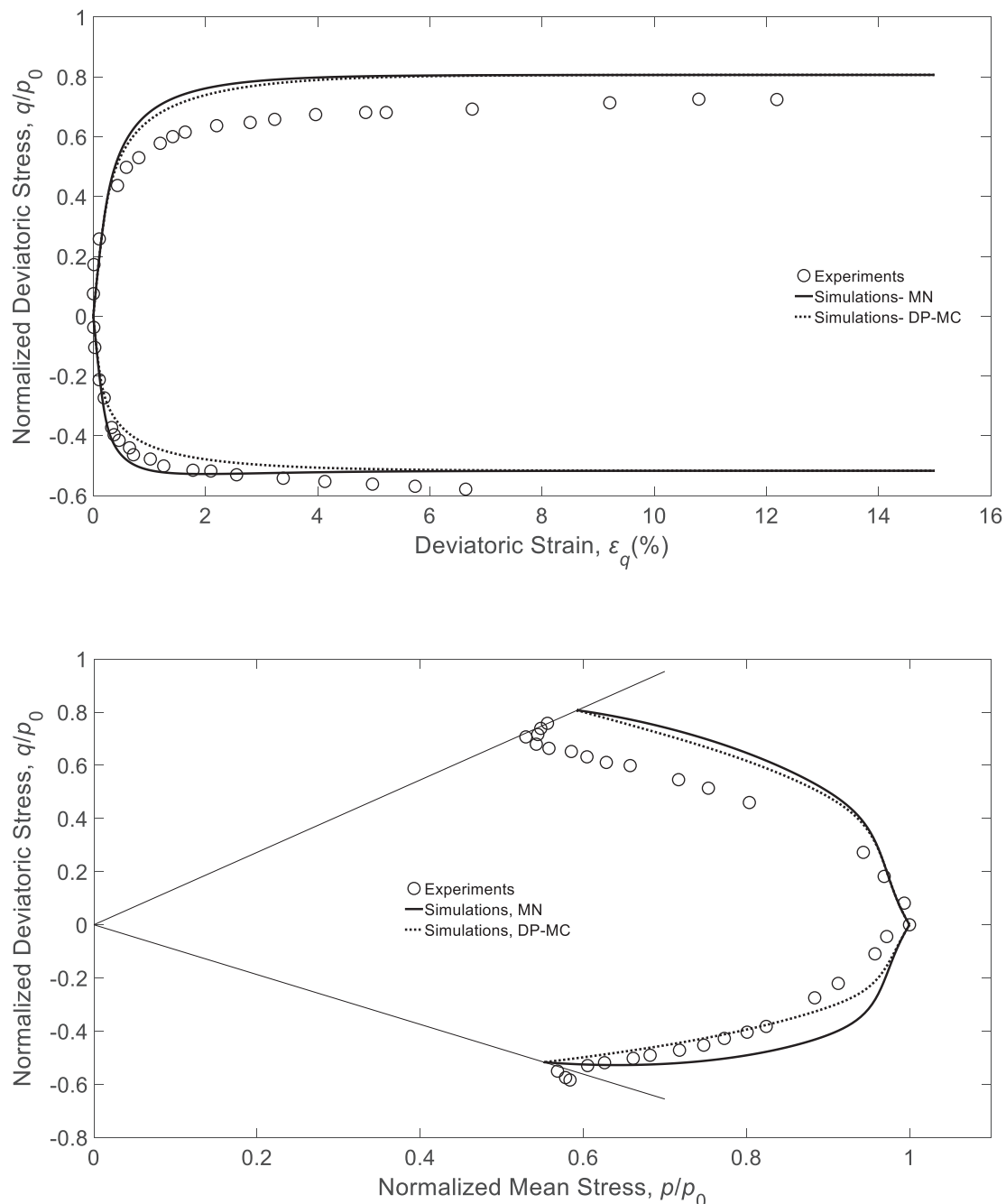
Fig. 16. Comparison between experimental and simulated undrained triaxial compression tests on reconstituted HKMD with different *OCR* under constant axial strain rate of 1.5%/h in terms of (a) stress–strain behaviour and (b) stress path.

$$r = \frac{\dot{\varepsilon}^p_v\big|_{oed}}{3\frac{\partial p_{eq}}{\partial(tr(\chi))}\big|_{K_0}} = \frac{\mu}{\tau\left(3\frac{\partial p_{eq}}{\partial(tr(\chi))}\big|_{K_0}\right)} \tag{39}$$

where $\dot{\varepsilon}^p_v\big|_{oed}$ is replaced by its value according to the time resistance concept (Grimstad et al., 2010). $\tau = 24h$ is the reference age or time (not absolute) associated with the reference isotache r obtained based on the oedometer test. Note that, based on Ziegler orthogonality, $\chi = \boldsymbol{\sigma}$ must be applied to equation (39) under the axisymmetric K_0 condition, based on which the lateral or horizontal effective stress is equal to the multiplication of the axial or vertical effective stress and K_0 value. Also note that, here, K_0 value is not a characteristic material parameter. It is given by the model based on certain values for the material parameters presented in Table 1.

Fig. 15 illustrates the simulated and experimental results of un-drained triaxial tests conducted at constant strain loading rates of 0.15, 1.5, and 15%/h on the HKMD specimens. Before shearing, each sample was normally consolidated to isotropic effective stress of 400 kPa. As shown, the model's responses with DP-MC and MN friction criteria are almost identical for the undrained compression tests. However, for the undrained extension tests, the MN criterion gives a higher deviatoric and stress ratio throughout whole tests. This is consistent with the obser-vation of the shear mobilisation in the looser side of the critical state line in Fig. 2.

To assess the performance of the model for the denser (over-consolidated) states, the undrained triaxial tests with the strain rate of 1.5%/h on the specimens of HKMD with different over-consolidation ratios ($OCR = p/p_0$) are also simulated. According to Fig. 16, the MN criterion results in a lower deviatoric and stress ratio than the DP-MC

Fig. 17. Comparison between experimental and simulated undrained triaxial tests on normally consolidated reconstituted Fujinomori clay under constant axial strain rate of 3.3×10^{-2}%/h in terms of (a) stress–strain behaviour and (b) stress path.

criterion for high *OCRs* (*OCR* = 4, 8), supported by the observation made in Fig. 3.

For further evaluation of the model performance, particularly the stress-induced anisotropic friction mobilisation, the drained true triaxial tests with shear loadings under constant spherical stress and different Lode angles on normally consolidated Fujinomori clay are simulated. But beforehand, to examine whether the chosen value for the spacing ratio parameter (*R*) is proper, the undrained triaxial test on a normally consolidated ($p = p_0 = 196$ kPa) specimen of Fujinomori clay under strain loading rate of 3.3×10^{-2}%/h (Nakai and Matsuoka, 1986) is predicted. The value of parameter *R* is selected from its relationship with the critical state angle of shearing resistance proposed by Nakai and Matsuoka (1986). As shown in Fig. 17, the predictions with both friction criteria are satisfactory. The predicted results of the drained true triaxial

tests under constant p = 196 kPa and *OCR* = 1 are compared with the measured results in Fig. 18 in terms of the maximum principal stress ratio (σ_1/σ_3) and the volumetric strain against the principal strains. Fig. 18 indicates that the hyper-viscoplastic model with MN friction criterion generally provides a better prediction. It is seen from the figure that more significant differences in predicted response by the friction criteria happen at shear loadings other than axisymmetric compression and extension. As expected, based on Fig. 18 (a), the predicted responses by both friction criteria are almost the same for the axisymmetric compression (θ = -30°).

10. Conclusions

In the present study, a set of thermodynamically consistent
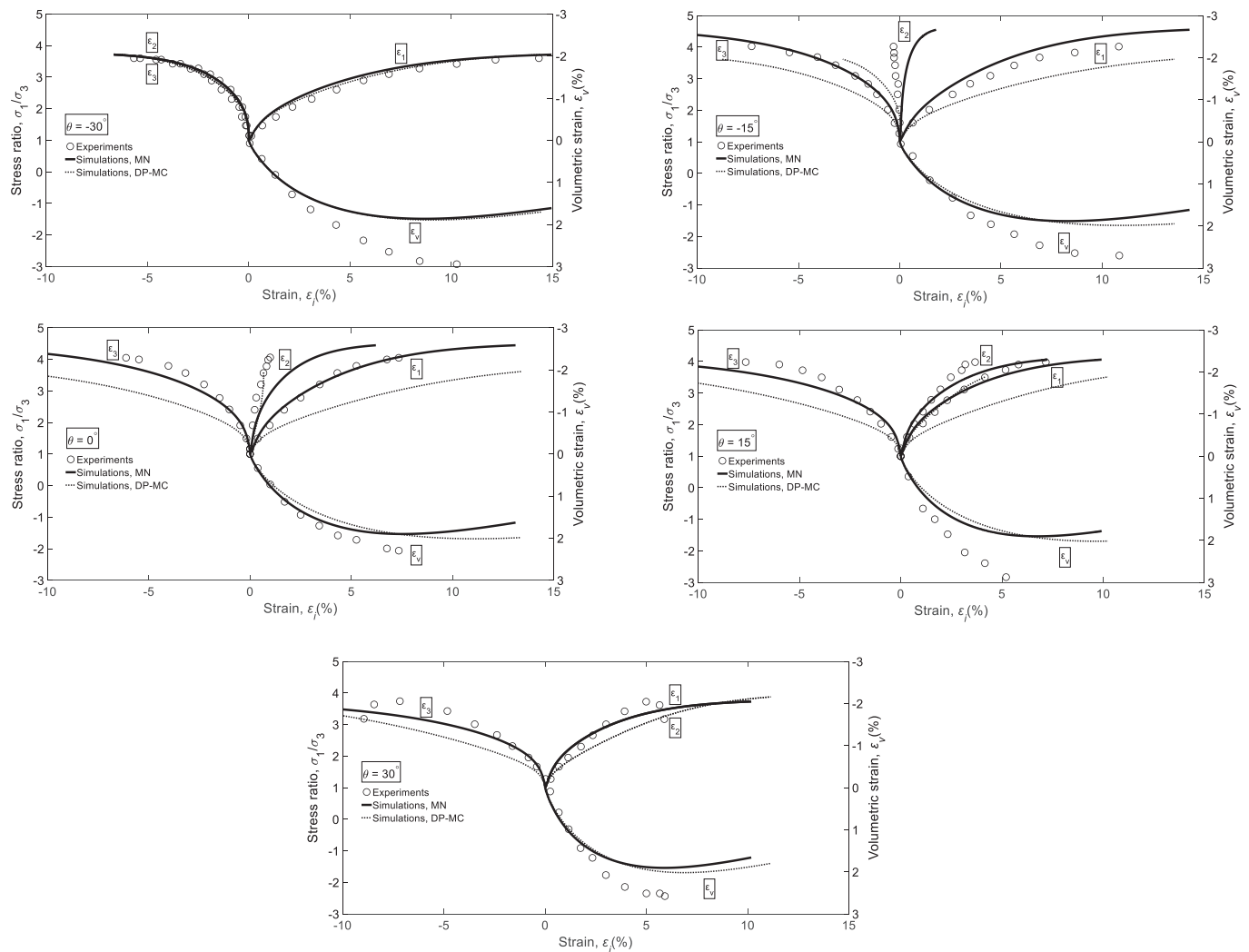
Fig. 18. Comparison between experimental and simulated drained true triaxial tests on normally consolidated reconstituted Fujinomori clay under different Lode angles of (a) −30°, (b) −15°, (c) 0°, (d) 15°, and (e) 30°.

viscoplastic models for clay has been constructed using the hyper-plasticity approach (Houlsby and Puzrin, 2007). The proposed models comply with the critical state soil mechanics (CSSM) theory (Schofield and Wroth, 1968) and the isotache viscosity (Leroueil, 2006, Suklje, 1957). Different friction criteria, namely the Drucker-Prager (DP), the Mohr-Coulomb (DP-MC) and the Matsuoka-Nakai (MN), have been employed. The features of the friction criteria in terms of friction mobilisation and inelastic flow direction in the meridian and the deviatoric stress space have been explored. Along this line, some interesting consistencies with DEM observations and insights have been reported and interpreted. It has been demonstrated that the model with the MN criterion exhibits a stress-induced anisotropic friction mobilisation, considered by a stress-coupled dissipative shearing mechanism that deviates from the stationary octahedral plane. This deviation is controlled by the stress ratio tensor ($\boldsymbol{\eta}$), which is an essential state variable of a particulate frictional system representing the degree of bimodal stress transmission. In addition, $\boldsymbol{\eta}$ has been tactfully used to obtain sets of hyper-viscoplastic models with a unique critical friction envelope, versatile dynamic surfaces, and non-associated flow rules. The fact that the proposed model exhibits a Lode angle-dependent behaviour similar to that observed in real experiments and the strong consistency of its stress–strain conjugate features (manifested by the hyperplasticity approach) with the results and insights gained via DEM studies in the literature suggest that the conjecture regarding the mesoscopic bimodal behaviour may have relevance to the behaviour of clays.

Another extension in this paper stemmed from the useful and universally employed first-order approximation of Coulomb's sliding friction being independent of the rate of the shearing process (Popova and Popov, 2015). This is ideally equivalent to the uniqueness of the critical friction envelope under different loading rates. In this regard, the conditions that cause non-uniqueness of the critical friction envelope for a rate-dependent particulate system with a single internal variable have been outlined. These conditions, which originate from the direct utilisation of the rate-independent formulations (e.g. Collins and Kelly (2002), Collins and Hilder (2002)) for rate-dependent cases (e.g. Jacquey and Regenauer-Lieb (2021)), are the existence of plastic free energy (leading to "shift or back stress" based on Ziegler's orthogonality postulate) or the frictional dissipation coupled with the internal variable in such a way that affects the homothetic viscosity.

The efficacy of the proposed model with the MN and the DP-MC friction criteria has been examined by simulating the conventional and true triaxial tests on Hong Kong Marine Deposits (HKMD) (Yin and Zhu, 1999, Zhu, 2000) and Fujinomori clay (Nakai and Matsuoka, 1986, Nakai et al., 1986). Overall, the hyper-viscoplastic model with MN friction criterion captures the behaviour of the clays better than the DP-MC friction. Although the MN criterion might not be considered a universal frictional criterion for different soils or even clay, its unique features and their consistency with DEM results highlight its structure as

a basis for the development of other forms or more general friction criteria using the thermodynamic-based approach of hyperplasticity.

Declaration of Competing Interest

The authors declare that they have no known competing financial interests or personal relationships that could have appeared to influence the work reported in this paper.

Appendix A. Thermodynamic rudiments

The infinitesimal strain hypothesis in the Cartesian coordinate system is adopted. Therefore, all extensive variables are considered as specific quantities in the forthcoming mathematics.

The hyperplasticity formalism emerges as a direct implementation of the thermodynamic laws. According to the first law, the universe's energy is constant. It can only change from one form to another by transferring between the system and its surroundings inside the universe. Generally, there are three mechanisms for transferring energy into and out of a system. Since the considered system is closed, no mass exchange with the surrounding can occur. Therefore, the first law can be mathematically expressed in its local form as:

$$\dot{u} = \sigma_{ij}\varepsilon_{ij} - q_{i,i} \tag{A-1}$$

stating that the internal energy (u) is generally changed by two forms of power input: the mechanical power and the heat supply per unit volume (written as the divergence of the heat flux vector q_i). Due to the transfer of mechanical and thermal power or energy, the phenomenological states of a system, quantified by deformation and temperature, can alter.

While the first law deals with the quantification and feasibility of the transfer of energy in thermal and mechanical forms, the second law introduces entropy (s) as a property of the system to identify the direction that energy tends to disperse naturally. Mathematically, the useful form for expressing the second law is the Clausius-Duhem inequality in the local form:

$$\dot{s} = -\left(\frac{q_i}{\theta}\right)_{,i} = -\frac{q_{i,i}}{\theta} + \left(\frac{\varsigma_i}{\theta}\right)\theta_{,i} \geqslant 0 \tag{A-2}$$

where θ and q_i/θ are temperature and the entropy flux (ς_i), respectively. By multiplying Equation (A-2) by θ, we have:

$$d = \theta\dot{s} + q_{i,i} - \varsigma_i\theta_{,i} \geqslant 0 \tag{A-3}$$

where d is the total dissipative power in the sense that the last term on the left-hand side of the inequality is known as the thermal dissipation, which is always non-negative since the heat flux is always in the opposite direction of the temperature gradient. The rest of the total dissipation can then be considered mechanical dissipation. The thermal dissipation is insignificant compared to the mechanical dissipation for slow processes (suited for the purpose of this paper), so it can be argued that, as a stronger statement, the mechanical dissipation must be non-negative (Houlsby and Puzrin, 2006). Moreover, the temperature gradient is zero for the isothermal condition (constant temperature). Therefore, by combining equations (A-1) and (A-3) we have:

$$\dot{u} + d = \sigma_{ij}\varepsilon_{ij} + \theta\dot{s} \tag{A-4}$$

subjected to $d \geq 0$. This equation is the starting point for developing the hyperplasticity formalism. But, Legendre transform is first introduced, to be able to have a more simplified perspective to equation (A-4) under isothermal condition.

Appendix B. Legendre transform

Legendre transform is essentially a method of transferring between potentials by interchanging the role of independent and dependent variables while pertaining all information and properties of the physical theory. More detailed account of this elegant mathematical tool can be found in Rockafellar (1997) and Houlsby and Puzrin (2006). The following briefly introduces some important properties of the Legendre transform.

Consider a potential function $X = X(x_1, \alpha)$. Only two independent variables, x_1 and α, are considered for simplicity. Since the function X acts as a potential, it can be written:

$$y_1 = \frac{\partial X(x_1, \alpha)}{\partial x_1} \tag{B-1}$$

where y_1 is the dependent variable conjugated to x_1. Here, we are interested in transforming X to the other form (Y, for example) in which the roles of x_1 and y_1 are interchanged; y_1 acts as an independent variable conjugated to x_1. Therefore, throughout the transformation, α serves as a passive variable. The $Y = Y(y_1, \alpha)$ can be defined via the Legendre transform:

$$Y(y_1, \alpha) = \pm[X(x_1, \alpha) - x_1y_1] \tag{B-2}$$

where the preference of sign is the matter of a particular application. It can be deduced that:

$$x_1 = \mp\frac{\partial Y}{\partial y_1} \tag{B-3}$$

$$\frac{\partial Y}{\partial \alpha} = \pm\frac{\partial X}{\partial \alpha} \tag{B-4}$$

Another important property of the Legendre transform is related to the scaling property of homogenous functions. Suppose X is a positive homogeneous function of the independent variable x_1 with the homogeneity order of m. By imposing Euler's theory for homogenous functions, it follows that Y is a positive homogeneous function of its independent variable y_1 (conjugated to x_1) with the homogeneity order of n such that:

$$\frac{1}{n} = \pm \left(\frac{1}{m} - 1 \right) \tag{B-5}$$

Appendix C. Hyperplasticity formalism

In the hyperplasticity approach, the state of a material element is characterised by a set of (internal) variables to capture the effect of the history. Internal variables are in addition to standard independent macroscopic state variables like strain or true stress. For the purpose of this paper, a single kinematic internal variable in tensorial form is assumed that can be identified as the plastic strain. However, there can generally be more internal variables in different forms depending on the (irreversible) mechanism they are associated with. Therefore, following Houlsby and Puzrin (2006), the internal variable is denoted by α_{ij} herein. The meaning for notions of independent and dependent variables will be seen in the following.

Since the current state of the material quantifies the internal energy to represent the path independent property of the material (the capacity), it is conceived as a function of independent state and internal variables, i.e., $u(\varepsilon_{ij}, \alpha_{ij}, s)$. Therefore, the rate of change of the internal energy can be given as:

$$\dot{u} = \left(\frac{\partial u}{\partial \varepsilon_{ij}} \right) \dot{\varepsilon}_{ij} + \left(\frac{\partial u}{\partial \alpha_{ij}} \right) \dot{\alpha}_{ij} + \left(\frac{\partial u}{\partial s} \right) \dot{s} \tag{C-1}$$

On the other hand, to describe the dissipative processes, Ziegler (1983) postulated that instead of treating the dissipation d in equation (A-4) as secondary importance (like the non-negativity checkpoint), d must be a primary function describing the dissipative power. Since dissipation is essentially path and history-dependent, the dissipation function (d) must be a function of rates of the internal variable. Since dissipative power is always non-negative based on the second law, any function for d cannot be a state function of its primary variable. Further, Ziegler (1983) postulated that the dissipation function d must be a positively homogenous or pseudo-homogeneous function of rates of internal variables. Based on Euler's theorem, for a positively homogeneous dissipation function of order n, there is:

$$d = \frac{1}{n} \left(\frac{\partial d}{\partial \dot{\alpha}_{ij}} \right) \dot{\alpha}_{ij} = \left(\frac{\partial z}{\partial \dot{\alpha}_{ij}} \right) \dot{\alpha}_{ij} \tag{C-2}$$

where $z = d/n$, which is called force potential (more detail provided in the following). For the particular case of rate-independent dissipative behaviour, n is one, and d equals z. Throughout this paper, the general form of homogeneity for d is invoked since the rate independency is not the prime subject of this paper. The homogeneity or pseudo-homogeneity of d is a powerful postulate that reciprocally is linked to the fundamental definition of power (here is a dissipative power) if d exists as a primary function of the rate of internal variables. This importance leads not only to the determination of the thermodynamic dissipative stresses conjugated to the rate of internal variables but also to maximising the dissipation rate. More details regarding the maximum dissipation are provided in the next section. It should be emphasised that the dissipation or the force potential can also be a function of state and internal variables. However, the role of these variables would be passive.

Having established the rates of change of the internal energy and dissipation, equation (A-4) can hence be extended by replacing equations (C-1) and (C-2), and grouping each rate terms:

$$\left(\frac{\partial u}{\partial \varepsilon_{ij}} - \sigma_{ij} \right) \dot{\varepsilon}_{ij} + \left(\frac{\partial u}{\partial s} - \theta \right) \dot{s} + \left(\frac{\partial u}{\partial \alpha_{ij}} + \frac{\partial z}{\partial \dot{\alpha}_{ij}} \right) \dot{\alpha}_{ij} = 0 \tag{C-3}$$

Now since entropy and strain are state variables and subsequently their rates are arbitrary at any thermodynamic state (free variation), for a pure reversible heating process in which $\dot{\varepsilon}_{ij}$ and $\dot{\alpha}_{ij}$ are both zero, one can deduce that:

$$\frac{\partial u}{\partial s} = \theta \tag{C-4}$$

Equation (C-4) demonstrates an example for the notion of dependent and independent variables. As the equation indicates, the temperature is a dependent variable since it can be derived by differentiating the potential function u in terms of the conjugated, independent variable entropy. So, one can apply the Legendre transform to interchange the role of these variables and to obtain the other form of the free energy, the Helmholtz free energy (f):

$$f(\varepsilon_{ij}, \alpha_{ij}, \theta) = u(\varepsilon_{ij}, \alpha_{ij}, s) - \theta s \tag{C-5}$$

Now by practising the property of the Legendre transform for passive variables of ε_{ij} and α_{ij}, it can be obtained:

$$\frac{\partial f}{\partial \varepsilon_{ij}} = \frac{\partial u}{\partial \varepsilon_{ij}} \tag{C-6}$$

$$\frac{\partial f}{\partial \alpha_{ij}} = \frac{\partial u}{\partial \alpha_{ij}} \tag{C-7}$$

By replacing equations (C-4), (C-6), and (C-7) in equation (C-3), for an isothermal condition, we have:

$$\left(\frac{\partial f}{\partial \varepsilon_{ij}} - \sigma_{ij} \right) \dot{\varepsilon}_{ij} + \left(\frac{\partial f}{\partial \alpha_{ij}} + \frac{\partial z}{\partial \dot{\alpha}_{ij}} \right) \dot{\alpha}_{ij} = 0 \tag{C-8}$$

since the strain is a state variable, and f is state property, the strain rate is subsequently arbitrary at any thermodynamic state. Therefore, the following relation between stress–strain can be deduced:

$$\frac{\partial f}{\partial \varepsilon_{ij}} = \sigma_{ij} \tag{C-9}$$

However, the same conclusion as the above cannot be deduced for the second differential term in equation (C-8) because z is not a state function. The only conclusion is that the internal variable has no exclusive contribution to the free energy increase but only contributes to the increase of the dissipation (entropy production). To satisfy the last differential term, generally, two possibilities emerge:

$$\frac{\partial f}{\partial \alpha_{ij}} + \frac{\partial z}{\partial \dot{\alpha}_{ij}} = 0 \quad \text{or equivalently} \quad -\overline{\chi}_{ij} + \chi_{ij} = 0 \tag{C-10}$$

$$\left(\frac{\partial f}{\partial \alpha_{ij}} + \frac{\partial z}{\partial \dot{\alpha}_{ij}} \right)\dot{\alpha}_{ij} = 0 \quad \text{or equivalently} \quad \left(-\overline{\chi}_{ij} + \chi_{ij} \right)\dot{\alpha}_{ij} = \widetilde{\chi}_{ij}\dot{\alpha}_{ij} = 0 \tag{C-11}$$

where after Houlsby and Puzrin (2006), $\overline{\chi}_{ij}$ and χ_{ij} are called the generalised and dissipative stresses, respectively, to conveniently distinguish the non-dissipative and dissipative internal stresses that are both work-conjugated to the rate of the internal variable. $\overline{\chi}_{ij}$ is the conservative stress since it is derived from the internal energy potential. $\widetilde{\chi}_{ij}$ is called gyroscopic stress since $\widetilde{\chi}_{ij}$ is orthogonal to $\dot{\alpha}_{ij}$ resulting in zero power. Ziegler (1983) argues that phenomenologically, the gyroscopic stresses or forces are not present, particularly in the mechanics of continuum media. Therefore, Ziegler (1983) postulated the first alternative, the orthogonality condition, leading to the following system of equations in which the number of unknown variables (internal and dependent state variables) equal to the number of equations supplied by the two potentials without any side conditions:

$$\frac{\partial f}{\partial \varepsilon_{ij}} = \sigma_{ij}$$
$$\frac{\partial z}{\partial \dot{\alpha}_{ij}} = -\frac{\partial f}{\partial \alpha_{ij}} \tag{C-12}$$

Appendix D. Ziegler's orthogonality condition and maximum dissipation

This section, by following Ziegler (1983), demonstrates why Ziegler's postulate is an orthogonality condition leading to the maximum dissipation rate, which makes the postulate a stronger statement than the second law. To do so, no prerequisite assumptions and conditions regarding the form of the dissipation function are made. The only prerequisites are definite non-negativity of dissipation rate, and the fundamental postulate of power, here a dissipative power:

$$d\left(\dot{\alpha}_{ij}, r \right) = \chi_{ij}\dot{\alpha}_{ij} \tag{D-1}$$

in which d is a primary invariant entity, i.e., a primary function of the rate of internal variable as the primary variable. Note that χ_{ij} is not yet defined but only considered as a variable conjugated to $\dot{\alpha}_{ij}$. For generality, r is defined as a set of state and internal variables with the passive role. The above construction is essentially phenomenological and free from microscopic complexities. The fundamental postulate of power determines the dissipative stress (χ_{ij}) as the space of linear mappings taking elements of $\dot{\alpha}_{ij}$ into scalars of dissipative power, which imposes χ_{ij} to be so-called dual space of $\dot{\alpha}_{ij}$. Now, the task is to determine χ_{ij} in a way that maximises the dissipation (d) subjected to the constraint of the fundamental postulate of power. To do so, the following Lagrangian can be casted:

$$L = d + \Lambda\left(d - \chi_{ij}\dot{\alpha}_{ij} \right) \tag{D-2}$$

where Λ is the Lagrange multiplier. The extrema of d can be found by:

$$\frac{\partial L}{\partial \dot{\alpha}_{ij}} = \frac{\partial d}{\partial \dot{\alpha}_{ij}} + \Lambda\left(\frac{\partial d}{\partial \dot{\alpha}_{ij}} - \chi_{ij} \right) = 0 \tag{D-3}$$

which leads to the definition of χ_{ij} as:

$$\chi_{ij} = \left(\frac{1 + \Lambda}{\Lambda} \right)\frac{\partial d}{\partial \dot{\alpha}_{ij}} \tag{D-4}$$

This definition for χ_{ij} indicates that the dissipative stress is in the direction of the gradient of the dissipation function, like the deduction made from the homogeneity condition of d. By replacing this definition for χ_{ij} in equation (D-1), the dissipative power can be expressed as:

$$d\left(\dot{\alpha}_{ij}, r \right) = \chi_{ij}\dot{\alpha}_{ij} = \left(\frac{1 + \Lambda}{\Lambda} \right)\frac{\partial d}{\partial \dot{\alpha}_{ij}}\dot{\alpha}_{ij} \geqslant 0 \tag{D-5}$$

Considering that based on the second law, d must be non-negative definite and contain the origin $\left(\dot{\alpha}_{ij} = 0 \right)$, it can be deduced that d must be a differentiable convex surface of $\dot{\alpha}_{ij}$, that is maximised by the definition of χ_{ij} in equation (D-4) obtained based on the extremum principle. Since χ_{ij} is orthogonal to the level set of d, this result is known as Ziegler's orthogonality postulate. By combining equations (D-4) and (D-5), the dissipative stress can be expressed solely based on the dissipation function:

$$\chi_{ij} = \left(\frac{d}{\frac{\partial d}{\partial \dot{\alpha}_{ij}} \dot{\alpha}_{ij}} \right) \frac{\partial d}{\partial \dot{\alpha}_{ij}} \tag{D-6}$$

which in combination with the postulate of Ziegler (equation (C-10)), leads to the derivation of the complete response of a system, conservative or dissipative, just by the specification of two potential functions: u (or other dual forms like f) and d, while subscribing to the principle of maximum dissipation rate.

Appendix E. Force and flow potentials

It has been shown previously that the dissipative stress can be derived by derivation of the dissipation function with respect to the internal variable rate. As can be seen, based on Euler's theorem for homogenous functions of order n, the scaling factor inside the parenthesis in equation (D-6) is equal to $1/n$. For rate-independent material, n is unity, and as a result, the dissipative stress can be purely derived from the derivation of the dissipation function:

$$\chi_{ij} = \frac{\partial d}{\partial \dot{\alpha}_{ij}} \tag{E-1}$$

in this case, d serves as a potential for the dissipative stress and provides a derivation relationship between independent (rate of the internal variable) and dependent variables (dissipative stress). However, for the rate-dependent material, which is of interest, with a homogenous dissipation function of order n, the dissipative stress can be derived as:

$$\chi_{ij} = \left(\frac{1}{n} \right) \frac{\partial d}{\partial \dot{\alpha}_{ij}} \tag{E-2}$$

This definition for χ_{ij} indicates that the dissipation function does not act as an potential but rather as a pseudopotential (Houlsby and Puzrin, 2002). By introducing the force potential as $z = d/n$, the dissipative stress can then be obtained by:

$$\chi_{ij} = \frac{\partial z}{\partial \dot{\alpha}_{ij}} \tag{E-3}$$

which indicates that z is a potential for dissipative stresses. Therefore, z, which working with provides a neat formulation free from ubiquitous homogeneity order, was called the force potential previously. Now, a Legendre transformation can be made to interchange the role of the dependent and independent variables and identify the flow potential w:

$$w\left(\chi_{ij}, \sigma_{ij}, \alpha_{ij} \right) = \chi_{ij}\dot{\alpha}_{ij} - z\left(\dot{\alpha}_{ij}, \sigma_{ij}, \alpha_{ij} \right) = d\left(\dot{\alpha}_{ij}, \sigma_{ij}, \alpha_{ij} \right) - z\left(\dot{\alpha}_{ij}, \sigma_{ij}, \alpha_{ij} \right) \tag{E-4}$$

where it can be deduced:

$$\dot{\alpha}_{ij} = \frac{\partial w}{\partial \chi_{ij}} \tag{E-5}$$

which means that w is a potential for the rate of the internal variable with a resemblance to the dynamic yield surface in the overstress viscoplastic theory of Perzyna (1963). The flow potential is a useful form of a dissipative potential for the conventional numerical implementation as it can readily be invoked in the strain-based incremental formulation. Based on the scaling property of Legendre type functions, since z is a positive homogenous function of order n in terms of $\dot{\alpha}_{ij}$, w is a positive homogenous function of order m in terms of χ_{ij} such that:

$$\frac{1}{m} + \frac{1}{n} = 1 \tag{E-6}$$

if z is a first order homogenous function of $\dot{\alpha}_{ij}$, then $z = d$ and $w = 0$. In this case, w is similar to the yield function. To obtain w from d in this case, the degenerate form of Legendre transform (Collins and Houlsby, 1997b) or the convex analysis (Srinivasa, 2010, Houlsby and Puzrin, 2006) can be employed.

Appendix F. Switch from the force potential to the flow potential suited for the Matsuoka-Nakai frictional criterion

The force potential can be specified as:

$$z = \left(\frac{1}{n} \right) \left(\frac{r^{1-n}p_0}{2^n} \right) \left(\sqrt{\text{tr}^2(\dot{\boldsymbol{\varepsilon}}^{\mathbf{p}}) + \left(M_{\mathbf{SMP}}\dot{\varepsilon}_{\mathbf{s}}^{\mathbf{p}} \right)^2} + \text{tr}(\dot{\boldsymbol{\varepsilon}}^{\mathbf{p}}) \right)^n \tag{F-1}$$

where $\dot{\varepsilon}_s^p = \sqrt{3}\dot{\varepsilon}_{s,DKP}^p$ is the shear strain rate measure on the dual kinematic plane (Collins, 2003):

$$\dot{\varepsilon}_{s,DKP}^p = \frac{\sqrt{\text{tr}(\boldsymbol{\sigma})\text{tr}\left(\boldsymbol{\sigma}.\left({}^{D}\dot{\boldsymbol{\varepsilon}}^{\mathbf{p}} \right)^2 \right) - \left(\text{tr}(\boldsymbol{\sigma}.\ {}^{D}\dot{\boldsymbol{\varepsilon}}^{\mathbf{p}}) \right)^2}}{\text{tr}(\boldsymbol{\sigma})} \tag{F-2}$$

All other parameters and variables in equation (F-1) are the same as equation (5). Therefore, the corresponding spherical and deviatoric components of the dissipative stress (χ) can be computed as:

$$\chi_p = \frac{\mathrm{tr}(\boldsymbol{\chi})}{3} = \frac{\partial z}{\partial(\mathrm{tr}(\dot{\boldsymbol{\varepsilon}}^p))} = \left(\frac{1}{2}\right)\left[p_0\left(\frac{zn}{r}\right)^{n-1}\right]^{\frac{1}{n}}\left(\frac{\mathrm{tr}(\dot{\boldsymbol{\varepsilon}}^p)}{\sqrt{\mathrm{tr}^2(\dot{\boldsymbol{\varepsilon}}^p)+\left(\mathrm{M_{SMP}}\dot{\varepsilon}_s^p\right)^2}}+1\right) \tag{F-3}$$

$$^D\boldsymbol{\chi} = \frac{\partial z}{\partial\;^D\dot{\boldsymbol{\varepsilon}}^p} = \left(\frac{1}{2}\right)\left[p_0\left(\frac{zn}{r}\right)^{n-1}\right]^{\frac{1}{n}}3M_{SMP}^2\left(\frac{\mathrm{tr}(\boldsymbol{\sigma})\left(\frac{^D\dot{\varepsilon}^p.\boldsymbol{\sigma}+\boldsymbol{\sigma}.\quad^D\dot{\varepsilon}^p}{2}\right)-\mathrm{tr}(\boldsymbol{\sigma}.\quad^D\dot{\boldsymbol{\varepsilon}}^p)\boldsymbol{\sigma}}{\mathrm{tr}^2(\boldsymbol{\sigma})\sqrt{\mathrm{tr}^2(\dot{\boldsymbol{\varepsilon}}^p)+\left(\mathrm{M_{SMP}}\dot{\varepsilon}_s^p\right)^2}}\right) \tag{F-4}$$

By definition (equations (D-6) and (E-3)), $^D\boldsymbol{\chi}$ is work-conjugate to $^D\dot{\boldsymbol{\varepsilon}}^p$. However, to find the dual form of the force potential (the flow potential), we need to derive the dissipative stress work- conjugated to $\dot{\varepsilon}_s^p$. To do so, both sides of equation (F-4) are first squared and multiplied by $\boldsymbol{\sigma}^{-1}$. The trace of the outcome in both sides results in:

$$\mathrm{tr}\left(\boldsymbol{\sigma}^{-1}.(\quad^D\boldsymbol{\chi})^2\right) = \left(\left(\frac{1}{2}\right)\left[p_0\left(\frac{zn}{r}\right)^{n-1}\right]^{\frac{1}{n}}\right)^2\left(3M_{SMP}^2\right)^2\left(\frac{\mathrm{tr}(\sigma)\mathrm{tr}\left(\sigma.(\quad^D\dot{\varepsilon}^p)^2\right)-\mathrm{tr}^2\left(\sigma.\quad^D\dot{\varepsilon}^p\right)}{\mathrm{tr}^3(\sigma)\left(\sqrt{\mathrm{tr}^2(\dot{\varepsilon}^p)+\left(\mathrm{M_{SMP}}\dot{\varepsilon}_s^p\right)^2}\right)^2}\right) \tag{F-5}$$

Now by taking square root of both sides and constructing the definition of $\dot{\varepsilon}_{s,DKP}^p$ (equation (F-2)) on the right hand side, the stress χ_q work-conjugate to $\dot{\varepsilon}_s^p$ can be derived as:

$$\chi_q = \sqrt{p\,\mathrm{tr}\left(\boldsymbol{\sigma}^{-1}.(\quad^D\boldsymbol{\chi})^2\right)} = \left(\frac{1}{2}\right)\left[p_0\left(\frac{zn}{r}\right)^{n-1}\right]^{\frac{1}{n}}\left(\frac{M_{SMP}^2\dot{\varepsilon}_s^p}{\sqrt{\mathrm{tr}^2(\dot{\varepsilon}^p)+\left(\mathrm{M_{SMP}}\dot{\varepsilon}_s^p\right)^2}}\right) \tag{F-6}$$

where p is the spherical component of the true or Cauchy stress (σ). Now, having the dissipative stress measures computed, the following relation in terms of the conjugated measures of inelastic strain rate in the force potential can be casted:

$$\frac{\chi_q}{\chi_p} = \frac{M_{SMP}^2\dot{\varepsilon}_s^p}{\sqrt{\mathrm{tr}^2(\dot{\varepsilon}^p)+\left(\mathrm{M_{SMP}}\dot{\varepsilon}_s^p\right)^2}+\mathrm{tr}(\dot{\varepsilon}^p)} \tag{F-7}$$

rearranging this equation results in:

$$\frac{\dot{\varepsilon}_s^p}{\mathrm{tr}(\dot{\varepsilon}^p)} = \frac{2\left(\frac{\chi_q}{\chi_p}\right)}{M_{SMP}^2-\left(\frac{\chi_q}{\chi_p}\right)^2} \tag{F-8}$$

indicating that at the critical state:

$$\frac{\chi_q}{\chi_p} = M_{SMP} \tag{F-9}$$

Based on the definition provided in equation (E-4), the flow potential in terms of inelastic strain rate can be expressed as:

$$w = \left(\frac{n-1}{n}\right)\left(\frac{r^{1-n}p_0}{2^n}\right)\left(\sqrt{\mathrm{tr}^2(\dot{\boldsymbol{\varepsilon}}^p)+\left(\mathrm{M_{SMP}}\dot{\varepsilon}_s^p\right)^2}+\mathrm{tr}(\dot{\boldsymbol{\varepsilon}}^p)\right)^n \tag{F-10}$$

Now, by rearranging equation (F-3) and applying equation (F-8), the following relation can be obtained:

$$\left(\sqrt{\mathrm{tr}^2(\dot{\boldsymbol{\varepsilon}}^p)+\left(\mathrm{M_{SMP}}\dot{\varepsilon}_s^p\right)^2}+\mathrm{tr}(\dot{\boldsymbol{\varepsilon}}^p)\right)^{n-1} = \left(\frac{\chi_p}{p_0}\right)\left(\frac{2^n}{r^{1-n}}\right)\left(\frac{M_{SMP}^2+\left(\frac{\chi_q}{\chi_p}\right)^2}{2M_{SMP}^2}\right) \tag{F-11}$$

Applying this relation in equation (F-10) provides the flow potential in terms of the dissipative stress:

$$w = \left(\frac{n-1}{n}\right)(rp_0)\left(\frac{\chi_p}{p_0}\left(1+\left(\frac{\chi_q}{M_{SMP}\chi_p}\right)^2\right)\right)^{\frac{n}{n-1}} = \left(\frac{n-1}{n}\right)(rp_0)\left(\frac{p_{eq}}{p_0}\right)^{\frac{n}{n-1}} \tag{F-12}$$

in which:

$$\chi_q = \sqrt{p\,\mathrm{tr}\left(\boldsymbol{\sigma}^{-1}.(\quad^D\boldsymbol{\chi})^2\right)} \tag{F-13}$$

References

Adachi, T., Oka, F., Hirata, T., Hashimoto, T., Nagaya, J., Mimura, M., Pradhan, T.B.S., 1995. Stress-strain behavior and yielding characteristics of eastern osaka clay. Soils Found. 35 (3), 1–13.

Alonso-Marroquín, F., Luding, S., Herrmann, H.J., Vardoulakis, I., 2005. Role of anisotropy in the elastoplastic response of a polygonal packing. Phys. Rev. E 71 (5), 051304.

Amorosi, A., Rollo, F., Houlsby, G.T., 2020. A nonlinear anisotropic hyperelastic formulation for granular materials: comparison with existing models and validation. Acta Geotech. 15 (1), 179–196.

Antony, S.J., Kruyt, N.P., 2009. Role of interparticle friction and particle-scale elasticity in the shear-strength mechanism of three-dimensional granular media. Phys. Rev. E 79 (3), 031308.

Arulanandan, K., Shen, C.K., Young, R.B., 1971. Undrained Creep Behaviour of a Coastal Organic Silty Clay. Géotechnique 21 (4), 359–375.

Barreto, D., O'sullivan, C., 2012. The influence of inter-particle friction and the intermediate stress ratio on soil response under generalised stress conditions. Granul. Matter 14 (4), 505–521.

Bjerrum, L., 1967. Engineering Geology of Norwegian Normally-Consolidated Marine Clays as Related to Settlements of Buildings. Géotechnique 17 (2), 83–118.

Chang, C.S., Hicher, P.-Y., Yin, Z.Y., Kong, L.R., 2009. Elastoplastic Model for Clay with Microstructural Consideration. J. Eng. Mech. 135 (9), 917–931.

Chen, Y.N., Yang, Z.X., 2017. A family of improved yield surfaces and their application in modeling of isotropically over-consolidated clays. Comput. Geotech. 90, 133–143.

Collins, I.F., 2002. Associated and Non-Associated Aspects of the Constitutive Laws for Coupled Elastic/Plastic Materials. Int. J. Geomech. 2 (2), 259–267.

Collins, I.F., 2003. A systematic procedure for constructing critical state models in three dimensions. Int. J. Solids Struct. 40 (17), 4379–4397.

Collins, I.F., 2005. The concept of stored plastic work or frozen elastic energy in soil mechanics. Géotechnique 55 (5), 373–382.

Collins, I.F., Hilder, T., 2002. A theoretical framework for constructing elastic/plastic constitutive models of triaxial tests. Int. J. Numer. Anal. Meth. Geomech. 26 (13), 1313–1347.

Collins, I.F., Houlsby, G.T., 1997. Application of thermomechanical principles to the modelling of geotechnical materials. Proc. R. Soc. Lond. A 453 (1964), 1975–2001.

Collins, I.F., Kelly, P.A., 2002. A thermomechanical analysis of a family of soil models. Géotechnique 52 (7), 507–518.

Dadras-Ajirloo, D., Grimstad, G., Ghoreishianamiri, S.A., 2022. On the isotache viscous modelling of clay behaviour using the hyperplasticity approach. Géotechnique 1–43.

Dong, J., Turci, F., Jack, R.L., Faers, M.A., Royall, C.P., 2022. Direct imaging of contacts and forces in colloidal gels. J. Chem. Phys. 156 (21), 214907.

Drucker, D.C., 1959. A Definition of Stable Inelastic Material. J. Appl. Mech. 26 (1), 101–106.

Fleischmann, J.A., 2020. Micromechanical Exploration of the Lade-Duncan Yield Surface by the Discrete Element Method. Geotech. Geol. Eng. 38 (5), 5409–5431.

Gao, Z., Zhao, J., Yao, Y., 2010. A generalized anisotropic failure criterion for geomaterials. Int. J. Solids Struct. 47 (22), 3166–3185.

Grammatikopoulou, A., Zdravkovic, L., Potts, D.M., 2007. The effect of the yield and plastic potential deviatoric surfaces on the failure height of an embankment. Géotechnique 57 (10), 795–806.

Grimstad, G., Degago, S.A., Nordal, S., Karstunen, M., 2010. Modeling creep and rate effects in structured anisotropic soft clays. Acta Geotech. 5 (1), 69–81.

Grimstad, G., Mehli, M., Degago, S.A., 2015. Creep in clay during the first few years after construction. In: Deformation Characteristics of Geomaterials. IOS Press, pp. 915–922.

Grimstad, G., Dadrasajirlou, D., Amiri, S.a.G., 2020. Modelling creep in clay using the framework of hyper-viscoplasticity. Géotechnique Letters 10 (3), 404–408.

Grimstad, G., Long, M., Dadrasajirlou, D., Amiri, S.a.G., 2021. Investigation of Development of the Earth Pressure Coefficient at Rest in Clay During Creep in the Framework of Hyper-Viscoplasticity. Int. J. Geomech. 21 (1), 04020235.

Gutierrez, M., Ishihara, K., 2000. Non-Coaxiality and energy dissipation in granular materials. Soils Foundations 40 (2), 49–59.

Hattab, M., 2011. Critical state notion and microstructural considerations in clays. Comptes Rendus Mécanique 339 (11), 719–726.

Hattab, M., Chang, C.S., 2015. Interaggregate Forces and Energy Potential Effect on Clay Deformation. J. Eng. Mech. 141 (7), 04015014.

Hicher, P.Y., Wahyudi, H., Tessier, D., 2000. Microstructural analysis of inherent and induced anisotropy in clay. Mechanics of Cohesive-frictional Materials 5 (5), 341–371.

Houlsby, G.T., 1981. Study of plasticity theories and their applicability to soils. University of Cambridge, Cambridge, UK.

Houlsby, G.T., Amorosi, A., Rojas, E., 2005. Elastic moduli of soils dependent on pressure: a hyperelastic formulation. Géotechnique 55 (5), 383–392.

Houlsby, G.T., Puzrin, A.M., 2002. Rate-dependent plasticity models derived from potential functions. J. Rheol. 46 (1), 113–126.

Houlsby, G., Puzrin, A., 2006. Principles of Hyperplasticity: an Approach to Plasticity Theory Based on Thermodynamic Principles. Springer Verlag, London, p. 375.

Houlsby, G.T., Puzrin, A.M., 2007. Principles of hyperplasticity: an approach to plasticity theory based on thermodynamic principles. Springer Science & Business Media.

Houlsby, G. (2000) Critical state models and small-strain stiffness. In *Developments in Theoretical Geomechanics. Proceedings of the Booker Memorial Symposium.* (D. W Smith, andCarter, J. P. (eds)) Rotterdam, Netherlands; Brookfiels, VT: A.A. Balkema, Sydney, N.S.W., pp. 295-312.

Hurley, R.C., Hall, S.A., Andrade, J.E., Wright, J., 2016. Quantifying Interparticle Forces and Heterogeneity in 3D Granular Materials. Phys. Rev. Lett. 117 (9), 098005.

Jacquey, A.B., Regenauer-Lieb, K., 2021. Thermomechanics for Geological. Rock Mech Rock Eng 54 (10), 5355–5373.

Janbu, N., 1985. Soil models in offshore engineering. Géotechnique 35 (3), 241–281.

Janbu, N. (1969) The resistance concept applied to deformations of soils. In *Proceedings of the 7th International Conference on Soil Mechanics and Foundation Engineering.*), Mexico City, vol. 2529, pp. 191-196.

Jostad, H.P., Yannie, J., 2017. A procedure for determining long-term creep rates of soft clays by triaxial testing. Eur. J. Environ. Civ. Eng. 26 (7), 2600–2615.

Karapiperis, K., Harmon, J., Andò, E., Viggiani, G., Andrade, J.E., 2020. Investigating the incremental behavior of granular materials with the level-set discrete element method. J. Mech. Phys. Solids 144, 104103.

Kirkgard, M.M., Lade, P.V., 1993. Anisotropic three-dimensional behavior of a normally consolidated clay. Can. Geotech. J. 30 (5), 848–858.

M. Kumruzzaman, J.-H. Y. (2012) Influence of the intermediate principal stress on the stress–strain–strength behaviour of a completely decomposed granite soil. *Géotechnique* **62(3)**:275-280.

Lade, P.V., Duncan, J.M., 1975. Elastoplastic Stress-Strain Theory for Cohesionless Soil. J. Geotech. Eng. Div. 101 (10), 1037–1053.

Lade, P.V., Musante, H.M., 1978. Three-Dimensional Behavior of Remolded Clay. J. Geotech. Eng. Div. 104 (2), 193–209.

Leroueil, S., 2006. The Isotache approach. Where are we 50 years after its development by Professor Šuklje? Prof. Šuklje's Memorial Lecture. In: Proc. 13th Danube Eur. Conf. on Geotech. Engng.), Ljubljana, pp. 55–88.

Liu, J., Zhou, W., Ma, G., Yang, S., Chang, X., 2020. Strong contacts, connectivity and fabric anisotropy in granular materials: A 3D perspective. Powder Technol. 366, 747–760.

Maeda, K., Hirabayashi, H. & Ohmura, A. (2006) Micromechanical influence of grain properties on deformation - Failure behaviours of granular media by DEM. In *Proceedings of the International Symposium on Geomechanics and Geotechnics of Particulate Media - Geomechanics and Geotechnics of Particulate Media.*), pp. 173-179.

Matsuoka, H., 1976. On the significance of the "spatial mobilized plane". Soils Found. 16 (1), 91–100.

Matsuoka, H., 2006. The SMP concept-based 3D constitutive models for geomaterials. CRC Press.

Matsuoka, H., Nakai, T., 1974. Stress-deformation and strength characteristics of soil under three different principal stresses. Proc. Japan Soc. Civil Eng. 1974 (232), 59–70.

Nakai, T., 2007. Modeling of soil behavior based on tij concept. In: Proc. of 13th ARCSMGE, Keynote Paper.), Kolkata, India, pp. 69–89.

Nakai, T., 2012. Constitutive modeling of geomaterials: principles and applications. CRC Press.

Nakai, T., Matsuoka, H., 1986. A Generalized Elastoplastic Constitutive Model for Clay in Three-Dimensional Stresses. Soils Found. 26 (3), 81–98.

Nakai, T., Mihara, Y., 1984. A New mechanical quantity for soils and its application to elastoplastic constitutive models. Soils Foundations 24 (2), 82–94.

Nakai, T., Matsuoka, H., Okuno, N., Tsuzuki, K., 1986. True Triaxial Tests on Normally Consolidated Clay and Analysis of the Observed Shear Behavior Using Elastoplastic Constitutive Models. Soils Found. 26 (4), 67–78.

Oda, M., 1993. Inherent and induced anisotropy in plasticity theory of granular soils. Mech. Mater. 16 (1), 35–45.

Panteghini, A., Lagioia, R., 2018. An extended modified Cam-Clay yield surface for arbitrary meridional and deviatoric shapes retaining full convexity and double homothety. Géotechnique 68 (7), 590–601.

Perzyna, P., 1963. The constitutive equations for rate sensitive plastic materials. Q. Appl. Math. 20 (4), 321–332.

Phusing, D., Suzuki, K., Srirat, P., 2017. Evolutions of Fabric and Contact Forces of Granular Materials Under Continuously Varying b Value Using DEM.). Springer Singapore, Singapore, pp. 81–90.

Popova, E., Popov, V.L., 2015. The research works of Coulomb and Amontons and generalized laws of friction. Friction 3 (2), 183–190.

Potts, D.M., Gens, A., 1984. The effect of the plastic potential in boundary value problems involving plane strain deformation. Int. J. Numer. Anal. Meth. Geomech. 8 (3), 259–286.

Pouragha, M., Kruyt, N.P., Wan, R., 2021. Non-coaxial plastic flow of granular materials through stress probing analysis. Int. J. Solids Struct. 222-223, 111015.

Prashant, A., Penumadu, D., 2004. Effect of Intermediate Principal Stress on Overconsolidated Kaolin Clay. J. Geotech. Geoenviron. Eng. 130 (3), 284–292.

Prashant, A., Penumadu, D., 2005a. Effect of Overconsolidation and Anisotropy of Kaolin Clay Using True Triaxial Testing. Soils Foundations 45 (3), 71–82.

Prashant, A., Penumadu, D., 2005b. A laboratory study of normally consolidated kaolin clay. Can. Geotech. J. 42 (1), 27–37.

Radjai, F., Azéma, E., 2009. Shear strength of granular materials. Eur. J. Environ. Civ. Eng. 13 (2), 203–218.

Radjai, F., Wolf, D.E., Jean, M., Moreau, J.-J., 1998. Bimodal Character of Stress Transmission in Granular Packings. Phys. Rev. Lett. 80 (1), 61–64.

Rockafellar, R.T., 1997. Convex analysis. Princeton University Press.

Roscoe, K.H., 1970. The Influence of Strains in Soil Mechanics. Géotechnique 20 (2), 129–170.

Roscoe, K. & Burland, J. (1968) On the generalized stress-strain behaviour of 'wet clay'. In *Engineering plasticity.* (Heyman, J., andLeckie, F. (eds)) Cambridge University Press, Cambridge, pp. 535-609.

Satake, M. (1982) Fabric tensor in granular materials. In: *Proceedings of Deformation and Failure of Granular Materials* (Vermeer, P. a. a. L., H. J. (ed)). Balkema, pp. 63-68.

Schofield, A.N., Wroth, P., 1968. Critical state soil mechanics. McGraw-hill London.

Sheahan, T.C., Ladd, C.C., Germaine, J.T., 1996. Rate-Dependent Undrained Shear Behavior of Saturated Clay. J. Geotech. Eng. 122 (2), 99–108.

Shi, J., Guo, P., 2018a. Fabric evolution of granular materials along imposed stress paths. Acta Geotech. 13 (6), 1341–1354.

Shi, J., Guo, P., 2018b. Induced fabric anisotropy of granular materials in biaxial tests along imposed strain paths. SOILS AND FOUNDATIONS 58 (2), 249–263.

Shirmohammadi, A., Hajialilue-Bonab, M., Dadras-Ajirloo, D., 2021. Application of a Simplified Anisotropic Constitutive Model for Soft Structured Clay on Embankment Failure. Int. J. Geomech. 21 (8), 04021125.

Srinivasa, A.R., 2010. Application of the maximum rate of dissipation criterion to dilatant, pressure dependent plasticity models. Int. J. Eng. Sci. 48 (11), 1590–1603.

Suklje, L., 1957. The analysis of the consolidation process by the isotaches method. In: Proc. 4th Int. Conf. Soil Mech. Found. Engng.), London, pp. 319–326.

Tafili, M., Wichtmann, T., Triantafyllidis, T., 2021. Experimental investigation and constitutive modeling of the behaviour of highly plastic Lower Rhine clay under monotonic and cyclic loading. Can. Geotech. J. 58 (9), 1396–1410.

Thornton, C., 2000. Numerical simulations of deviatoric shear deformation of granular media. Géotechnique 50 (1), 43–53.

Thornton, C., Zhang, L., 2010. On the evolution of stress and microstructure during general 3D deviatoric straining of granular media. Géotechnique 60 (5), 333–341.

Topolnicki, M., Gudehus, G., Mazurkiewicz, B.K., 1990. Observed stress–strain behaviour of remoulded saturated clay under plane strain conditions. Géotechnique 40 (2), 155–187.

Vaid, Y.P., Campanella, R.G., 1977. Time-Dependent Behavior of Undisturbed Clay. J. Geotech. Eng. Div. 103 (7), 693–709.

Van Eekelen, H.A.M., 1980. Isotropic yield surfaces in three dimensions for use in soil mechanics. Int. J. Numer. Anal. Meth. Geomech. 4 (1), 89–101.

Vinutha, H.A., Diaz Ruiz, F.D., Mao, X., Chakraborty, B., Del Gado, E., 2023. Stress–stress correlations reveal force chains in gels. J. Chem. Phys. 158 (11), 114104.

Wan, R., Pinheiro, M., 2014. On the validity of the flow rule postulate for geomaterials. Int. J. Numer. Anal. Meth. Geomech. 38 (8), 863–880.

Ye, G.-L., Ye, B., Zhang, F., 2014. Strength and Dilatancy of Overconsolidated Clays in Drained True Triaxial Tests. J. Geotech. Geoenviron. Eng. 140 (4), 06013006.

Yin, J.-H., Zhu, J.-G., 1999. Measured and predicted time-dependent stress-strain behaviour of Hong Kong marine deposits. Can. Geotech. J. 36 (4), 760–766.

Yong, R.N., Mckyes, E., 1971. Yield and Failure of a Clay under Triaxial Stresses. J. Soil Mech. Found. Division 97 (1), 159–176.

Zhang, Z., Chen, Y., Huang, Z., 2018. A novel constitutive model for geomaterials in hyperplasticity. Comput. Geotech. 98, 102–113.

Zhou, W., Yang, S., Liu, J., Ma, G., Qi, T., Lin, M., 2021. Effect of inter-particle friction on 3D accordance of stress, strain, and fabric in granular materials. Acta Geotech. 17 (7), 2735–2750.

Zhu, J.-G., 2000. Experimental study and elastic visco-plastic modelling of the time-dependent stress-strain behaviour of Hong Kong marine deposits. vol. Ph.D Dept. of Civil and Structural Engineering. Hong Kong Polytechnic University, Hung Hom, Hong Kong.

Ziegler, H., 1983. An introduction to thermomechanics, 2nd edn. North-Holland, Amsterdam.